



**University of Kerbala**  
**College of Science**  
**Department of Chemistry**

**A study the Optical and Electrochemical Properties of  
Polyoxometalate -Based Non-Linear Optical Compounds.**

**A Thesis**

**Submitted to the Council of the College of Science University of Kerbala, in  
Partial Fulfilment of the Requirement for the Master Degree of  
Science in Chemistry**

**By**

**Ashraf Hussein Saleh**

**Supervised by**

**Asst. Prof. Dr.  
Ahmed Hadi Al-Yasari**

**Asst. Prof. Dr.  
Hasan Faisal Alesary**

**2023 A.D**

**1444 H.D**

بِسْمِ اللّٰهِ الرَّحْمٰنِ الرَّحِیْمِ

يَا أَيُّهَا الَّذِينَ آمَنُوا إِذَا قِيلَ لَكُمْ تَسَسَّخُوا فِي الْمَجَالِسِ فَافْسَحُوا يَفْسَحِ اللَّهُ لَكُمْ  
وَإِذَا قِيلَ انشُرُوا فَانشُرُوا يَرْفَعِ اللَّهُ الَّذِينَ آمَنُوا مِنْكُمْ وَالَّذِينَ أُوتُوا الْعِلْمَ دَرَجَاتٍ  
۝ وَاللَّهُ بِمَا تَعْمَلُونَ خَبِيرٌ

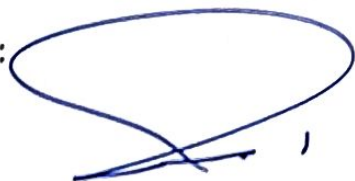
صدق الله العظيم

سورة المجادلة: آية ١١

## Supervisor Certification

We certify that this thesis was prepared by "Ashraf Hussein Saleh" my supervision at the Chemistry Department, Coll of Science, University Karbala, as a partical requirement for the degree of master of Science in Chemistry.

Signature:



Name: **Dr. Ahmed Hadi Al-Yasari**  
Title: Assistant Professor  
Address: University of Kerbala,  
College of Science,  
Department of Chemistry  
Date: / / 2023  
(Member & Supervisor)

Signature:



Name: **Dr. Hasan Faisal Alesary**  
Title: Assistant Professor  
Address: University of Kerbala,  
College of Science,  
Department of Chemistry  
Date: / / 2023  
(Member & Supervisor)

In view of the available recommendations by the Supervisor, I Forward this thesis for debate by the examining committee.

Signature:



Name: **Dr. Luma M. Ahmed**  
Title: Professor  
Head of Chemistry, College of Science,  
Date: 25/6 / 2023

## Examination Committee Certification

We certify that we have read this thesis entitled " A study the Optical and Electrochemical Properties of Polyoxometalate-Based Non-Linear Optical Compounds " As the examining committee, examined the student " Ashraf Hussein Saleh " on its contents, and that in our opinion, it is adequate for the partial fulfillment of the requirements for the Degree of Master in Science of chemistry.

Signature:



Name: **Dr. Eman Talib Kareem**

Title: Professor

Address: University of Kerbala, College of Science,  
Department of Chemistry.

Date: 25/6/2023

(Chairman)

Signature



Name: **Dr. Heider Abdulrazzaq Abdulhussein**

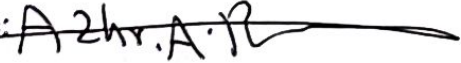
Title: Assistant Professor

Address: University of Kufa, College of  
Science, Department of Chemistry

Date: 5/6/2023

(Member)

Signature:



Name: **Dr. Azhr Abdulzahraa Raheem**

Title: Assistant Professor

Address: University of Kerbala, College of  
Science, Department of physics

Date: 25/6/2023

(Member)

Signature:



Name: **Dr. Ahmed Hadi Al-Yasari**

Title: Assistant Professor

Address: University of Kerbala, College of  
Science, Department of Chemistry

Date: 25/6/2023

(Member & Supervisor)

Signature:



Name: **Dr. Hasan Faisal Alesary** Title:

Assistant Professor

Address: University of Kerbala, College of  
Science, Department of Chemistry

Date: 25/6/2023

(Member & Supervisor)

Approved by the council of the College of Science

Signature:



Name: **Dr. Jasem Hanoon Hashim Al-Awadi**

Title: Professor

Address: **Dean of College of Science, University of Kerbala**

Date: 4/7/2023

*This thesis is dedicated  
to my father's Soul*

**HUSSEIN SALEH**

*Your Son*

*Ashraf*

## Acknowledgements

In the beginning, I would like to thank Allah for His blessings...

I would like to thank my supervisors, **Asst. Prof. Dr. Ahmed Hadi Al-Yasari**, for his guidance, inspiration and friendship over the duration of this research, with particular thanks to **Asst. Prof. Dr. Hasan Fisal Alesary** for his day-by-day guidance and supporting help during my research and writing this thesis.

I also extend my heartfelt thanks whoever help me from the teaching staff at the University of Kerbala, College of science, Department of chemistry.

I would like to express my deep appreciation to all of members my family and friends for their material and spiritual support.

## Abstract

This thesis is divided into three sections: the first includes an introduction to NLO materials and how to generate SHG with an explanation of the connection between the donor and the acceptor and the link between them through  $\pi$ -bridges by the Two-State Model. POM with its types was also discussed, and the most powerful donor that exists, which is julolidine, was also clarified. In the second section, the Schrödinger equation, the four approximations, what quantum chemistry is, and what is HF were explained, after which TDDFT, DFT, and related topics were discussed. In the third section was a discussion of all the results obtained.

Non-linear optical (NLO) materials are used to manipulate laser light through 2<sup>nd</sup> order phenomena such as second harmonic generation (frequency doubling), and 3<sup>rd</sup> order effects for instance multi-photon absorption. In this thesis, investigating of NLO materials in which polyoxometalate (POM) electron acceptors is connected via phenylimido groups to organic electron donors is conducted. In this project, we have theoretically, mostly by DFT calculations, systematically studied new compound such as julolidine-based donor groups, very strong donors, as an efficient NLO compound. Their geometric and electronic structures, linear optical and second-order nonlinear properties have also been evaluated. By the introduction of julolidine into the organoimido-hexamolybdate, the studied systems show substantial second-order nonlinear (NLO) responses of up to  $1048 \times 10^{-30}$  esu for compound **3**. Upon enlarging the  $\pi$ -conjugated linker, the calculated  $\beta$ -responses are enhanced by a factor of 2.1. Substitution effects (including alkyl and phenyl groups) on donor strength of julolidine and hence on the  $\beta$ -responses have also been investigated. The results showed an enhancement of up to 1.2 in  $\beta$ -responses for phenyl-substituted julolidine derivatives of up to  $1242 \times 10^{-30}$  esu for compound **8**.

In general, TD-DFT calculations indicate that the strong low-energy transition can mainly be attributed to charge transfer (CT) from julolidine-arylimido to the hexamolybdate cluster, indicating strong communication between the POM and julolidine components, which is responsible for the linear and non-linear optical behavior of these compounds. Ortho-methylation to the imido-bond has a significant effect on the stability and hence on the length and linearity of the bond, although it slightly reduces the first hyperpolarizability. The whole set of results demonstrates the excellent NLO activity for julolidine-POMs compound while keeping relatively good transparency window compared to similar purely organic systems.



## List of Abbreviations

Symbol	Definition
<i>A</i>	Acceptor
<i>B</i>	Field magnetic
BLA	Bond Length Alternation
BS	Basis Sets
CC	Coupled Cluster
CI	Configuration Interaction
CT	Charge-Transfer
D	Donor
DAST	Dimethyl-Amino-Stilbazolium Tosylate
DFM	Difference Frequency Mixing
DFT	Density Functional Theory
DH	Double Hybrid
DZ	Double Zeta
<i>E</i>	Field electrical
ECP	Effective Core Potentials
EESs	Electrical Energy Storages
$E_{\max}$	Optical transition energy between ground and excited state
EO	Electro-Optical
FMRs	Fluorescent Molecular Rotors
FMs	Functional Modules
GGA	Generalized Gradient Approximation
GTO	Gaussian Type Orbital
HF	Hartree-Fock
HOMO	High Energy Occupied Molecular Orbitals
HRS	Hyper-Raleigh Scattering

ICT	Intramolecular Charge-Transfer
ICTL	Intermolecular Charge Transfer Layers
LC	Long-Range Corrected
LMCT	Ligand to Metal Charge-Transfer
LUMO	Low Energy Unoccupied Molecular Orbitals
MBPT	Many-Body Perturbation Theory
MLCT	Metal to Ligand Charge-Transfer
MNPs	Metal Nanoparticles
MOFs	Metal-Organic Frameworks
NLO	Non-Linear Optical
NOPs	Nonlinear Optical Properties
OLEDs	Organic Light Emitting Diode
OR	Optical Rectification
POH	Plasmonic organic hybrid
POMs	Polyoxometalates
QC	Quantum Chemistry
QZ	Quadruple Zeta
RR	Rectification Ratio
RS	Range Separated
SFG	Sum Frequency Generation
SHG	Second Harmonic Generation
SPR	Surface Plasmon Resonances
STOs	Slater Type Orbitals
TDDFT	Time-Dependent Density Functional Theory
THz	Terahertz
TZ	Triple Zeta
VOCs	Volatile Organic Compounds
$\alpha$	Linear polarizability

$\beta$	Second-order polarizability or the first hyperpolarizability
$\beta_0$	First hyperpolarizability
$\gamma$	Third-order polarizability
$\Delta\mu_{12}$	Dipole Moment Change
$\lambda$	Wavelength of the incident light (laser)
$\lambda_{\max}$	Wavelength at maximum absorption
X	Connected linearly
$\omega_1, \omega_2$	Optical frequency

### List of Tables

No.	Subject	Page
3.1	Selected structural parameters where distances are in (Å) and angles in (°) of the geometries of compounds 1–4.	42
3.2	Calculated first hyperpolarizabilities (au) of anions 1–4 in comparison with experimental and calculated data for compound 9.	44
3.3	Calculated maximum absorption wavelength ( $\lambda_{\max}$ ), oscillator strength ( $f_{os}$ ), electronic transition energy ( $E_{\max}$ ), and the percentage MO contribution.	48
3.4	Selected structural parameters where distances are in (Å) and angles in (°) of the geometries of compounds 5–8.	55
3.5	Calculated first hyperpolarizabilities (au) of anions 5–8 in comparison with experimental and calculated data for compound 9.	57
3.6	Calculated maximum absorption wavelength ( $\lambda_{\max}$ ), oscillator strength ( $f_{os}$ ), electronic transition energy ( $E_{\max}$ ), and the percentage MO contribution.	61

### List of Figures

No.	Subject	Page
1.1	Diagram illustrating the creation of induced polarization, which causes the frequency of the incoming light to double.	3
1.2	Second Harmonic Generation.	4

1.3	Ball-stick and polyhedral representations for three most common polyoxometalate structures. (a) Lindqvist anion: $[M_6O_{19}]^{X-}$ ; (b) $[\alpha-\{XO_4\}_yM_{12}O_{36}]_y^-$ : Keggin anion; (c) $[\alpha-\{XO_4\}_2M_{18}O_{54}]_z^-$ : Wells-Dawson structure.	15
1.4	Structure of Julolidine.	20
3.1	Optimized geometries in the solvent phase for anions 1-4. Gray = C, cyan = Mo, white = H, blue = N, and red = O.	43
3.2	UV-Vis spectrum calculated theoretically for 1,2,3,4 respectively	47
3.3	The molecular orbitals involved in significant transitions of 1.	50
3.4	The molecular orbitals involved in significant transitions of 2.	51
3.5	The molecular orbitals involved in significant transitions of 3.	52
3.6	The molecular orbitals involved in significant transitions of 4.	53
3.7	Excitation-induced charge density difference ( $\Delta r$ ) for key excited states of compounds 1–4 (isovalue = 0.0003 au; light/dark blue corresponds to positive/negative $\Delta r$ so that the excitation-induced electron transfer goes from dark to light blue).	54
3.8	Optimized geometries of 5-8 anions in the solvent phase. Gray = C, cyan = Mo, white = H, blue = N, and red = O.	56
3.9	UV-Vis spectrum calculated theoretically for 5,6,7,8 respectively	59
3.10	The molecular orbitals involved in significant transitions of 5.	63
3.11	The molecular orbitals involved in significant transitions of 6.	64
3.12	The molecular orbitals involved in significant transitions of 7.	66
3.13	The molecular orbitals involved in significant transitions of 8.	67
3.14	Excitation-induced charge density difference ( $\Delta r$ ) for key excited states of compounds 5–8 (isovalue = 0.0003 au; light/dark blue corresponds to positive/negative $\Delta r$ so that the excitation-induced electron transfer goes from dark to light blue).	69

## List of Schemes

No.	Subject	Page
1.1	Structure of Dimethylamino-N-methyl-4-stilbazolium tosylate (DAST).	10
3.1	Hexamolybdate-organoimido-Julolidine derivatives 1 to 8 investigated in this study.	41

<b>Subject</b>		
<b>Subject</b>		<b>Page</b>
Abstract		<b>II</b>
List of Abbreviations		<b>IV</b>
List of Tables		<b>VI</b>
List of Figures		<b>VI</b>
List of Schemes		<b>VIII</b>
<b>Chapter One</b>		
<b>Introduction</b>		
<b>No.</b>	<b>Subject</b>	<b>Page</b>
1.1	Non-linear Optics	1
1.1.1	Physical Background	1
1.1.2	Nonlinear Optical (NLO) history	3
1.1.2.1	Second Harmonic Generation (SHG)	3
1.1.2.2	The Two-State Model	6
1.1.3	NLO materials	7
1.1.3.1	Inorganic-based NLO Materials	7
1.1.3.2	Organic/Metallo-organic based NLO Materials	7
1.1.3.3	D- $\pi$ -A compound	12
1.1.4	NLO Switchable	13
1.2	Polyoxometalates (POMs)	13
1.2.1	Lindqvist-organoimido derivatives	16
1.2.2	Organoimido-Lindqvist as NLO materials - Literature review	18
1.3	Julolidine-based donors	20
1.4	Aim of Study	23

<b>Chapter 2</b>		
<b>Computational Theory and Method</b>		
<b>No.</b>	<b>Subject</b>	<b>Page</b>
2.1	Schrödinger Equation	24
2.2	Quantum Chemistry	26
2.3	Hartree-Fock Self Consistent Field	27
2.4	Electron Correlation	28
2.5	Density Functional Theory (DFT)	28
2.5.1	Time-Dependent Density Functional Theory (TDDFT)	31
2.5.2	$\omega$ B97XD	33
2.6	Basis Sets	33
2.6.1	LANL2TZ	36
2.7	Computational Chemistry	37
2.8	Computational Methods	38
2.8.1	Hyperpolarizability and Two-State Model Analysis	39
<b>Chapter 3</b>		
<b>Results and Discussions</b>		
<b>No.</b>	<b>Subject</b>	<b>Page</b>
3	RESULTS AND DISCUSSIONS	41
3.1	Ground-State Molecular Geometries For 1 to 4 Compounds	42
3.2	NLO Properties: First Hyperpolarizabilities For 1 to 4 Compounds	44
3.3	UV– Vis Absorption Spectra For 1 to 4 Compounds	45
3.4	Effects Of Substituents on Julolidine	55
3.4.1	Ground-State Molecular Geometries For 5 to 8 Compounds	55
3.4.2	NLO Properties: First Hyperpolarizabilities For 5 to 8 Compounds	57
3.4.3	UV–Vis Absorption Spectra For 5 to 8 Compounds	58
3.5	Conclusion	69

3.6	Future Works	70
<b>References</b>		



# **Chapter One**

## **Introduction**

## Chapter One

## Introduction

**1.1 Non-linear Optics:****1.1.1 Physical Background:**

Before describing the relationship between the ideas of "light" and "matter," it is crucial to comprehend these terms. On the basis of Maxwell's theory, light is made up the oscillating fields of two-electrical ( $E$ ) and magnetic ( $B$ ) that are perpendicular to one another directions of transmission and orthogonal to each other. Atoms, which have positively charged nuclei and negatively charged electrons, make up matter. When light interacts with a substance, the atom's electron density is displaced (polarized) by the electric field of the light ( $E$ ). As a result of this interaction, an induced dipole moment that oscillates at the same frequency as the applied light field is created. The induced electric-dipole moment and the electric field are connected linearly ( $\alpha$ ) when the intensity of the incoming light is relatively low (equation 1.1).

$$\text{Polarization} = \mu = \alpha E \quad (1.1)$$

The linear susceptibility ( $\chi$ ) of a group of molecules is utilized for bulk or macroscopic materials (equation 1.2).<sup>[1]</sup>

$$P = \chi E \quad (1.2)$$

All of material's optical characteristics, as well as associated processes like absorption, reflection, refraction, and diffusion, are described by the polarization, it emits radiation at that frequency and serves as a source. When the electric field of the light is high, the relationship between the induced dipole moments and the electric field is no longer linear, and the optical susceptibility ( $\chi$ ) varies on the applied electric field. Thus, a power series of the applied electric field may be used to express the polarization..<sup>[2]</sup>

$$\mathbf{P} = \mathbf{P}^L + \mathbf{P}^{NL} \quad (1.3)$$

$$\mathbf{P} = \chi^1 E + \chi^2 EE + \chi^3 EEE + \dots \quad (1.4)$$

or

$$\mu = \alpha E + \beta EE + \gamma EEE + \dots \quad (1.5)$$

Where  $\alpha$  is the linear polarizability,  $\beta$  is the second-order polarizability or the first hyperpolarizability, and  $\gamma$  is the third-order polarizability or the second hyperpolarizability. When a material with a second-order non-linear susceptibility is exposed to an optical field at two frequencies ( $\omega_1, \omega_2$ ), its non-linear polarization will act as a source of radiation at new frequencies,  $2\omega_1, 2\omega_2, \omega_1 + \omega_2$ , and  $|\omega_1 - \omega_2|$ . They describe the beginnings of non-linear phenomena like SHG, sum frequency generation (SFG), difference frequency mixing (DFM), and optical rectification (OR). In this dissertation, frequency doubling and SHG are the main topics shown in (Figure 1.1).

A third rank tensor with 27 non-independent parts makes up the first hyperpolarizability  $\beta$ , in which symmetry is essential. For instance, depending on the symmetry of the molecule, some of these 27 constituents vanish; for centrosymmetric materials, the initial hyperpolarizability, becomes zero. These 27 components are the many ways that the three Cartesian elements of polarization and the two interacting electric fields can be combined. These 27 elements may be reduced using molecular symmetry, so generally, just a few parts are non-zero. For all the molecules investigated in this Work, there is often just one component that is much bigger than the others, allowing us to ignore the rest and simplify the 27 tensors to just one component.

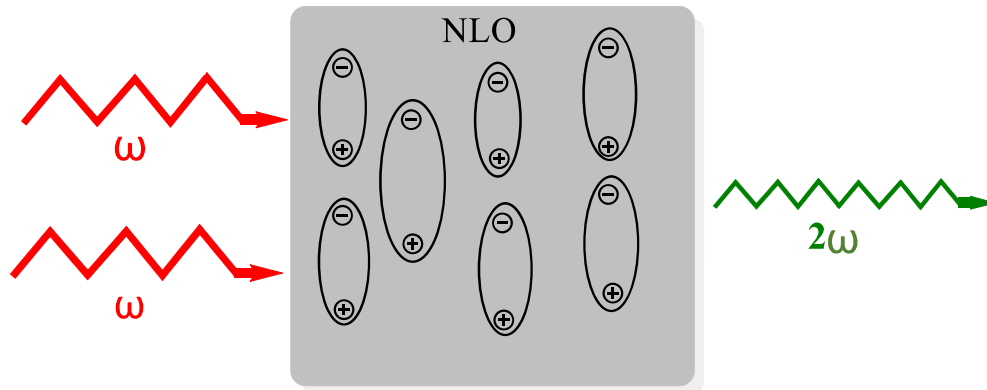


**Figure 1.1** Diagram illustrating the creation of induced polarization, which causes the frequency of the incoming light to double.

### 1.1.2 Nonlinear Optical (NLO) History:

NLO is the study of events that occur when the presence of light modifies the optical properties of a material system. Typically, only laser light is powerful enough to change a material system's optical characteristics. By Franken and others, the second-harmonic generation was discovered (1961)<sup>[3]</sup>, which came soon after Maiman's demonstration of the first functional laser in 1960,<sup>[4]</sup> It is occasionally considered to mark the beginning of the area of NLO. When a material system behaves nonlinearly depending on the intensity of an applied optical field, this is referred to as a NLO phenomenon. For instance, the portion of the atomic response that scales quadratically with the intensity of the applied optical field results in second-harmonic production. As a result, the second-harmonic light's intensity tends to rise in direct proportion to the intensity of the laser light that is being used.<sup>[2]</sup>

#### 1.1.2.1 Second Harmonic Generation (SHG):

SHG, which is recognized as a fundamental technique for optical frequency conversion in both quantum and classical optics, was discovered at the beginning of the key field of research known as second-order NLO. SHG was reported in 1961 by Franken et al. thrust the study of NLO materials into the centre of

attention of scientific inquiry<sup>[3]</sup>. In the five decades that followed, NLO saw a number of advancements, including novel NLO phenomena and a number of new applications. Numerous current optical data storage, holographic imaging, frequency mixing, telecommunications, and other fields might use the NLO materials. Over the past two decades, numerous attempts have been made to establish the fundamental ideas, identify novel NLO phenomena, create high-performance materials, and take advantage of NLO's applications.<sup>[5][6]</sup> The science of creating and perfecting NLO molecular materials has recently undergone a significant transformation thanks to theoretical chemistry techniques such as computational chemistry.

In second-order NLO, atoms and molecules are irradiated with an electric field that is equivalent to their interatomic field using lasers with high degrees of directionality, coherence, and spectrum purity. The second-order NLO process provides a fundamental framework for understanding laser-matter interactions, which paves the way for the use of NLO effects in a variety of technical fields, like optical communication, optical switching, and optical data storage. Therefore, designing and creating NLO materials has been an important area of study for many years.

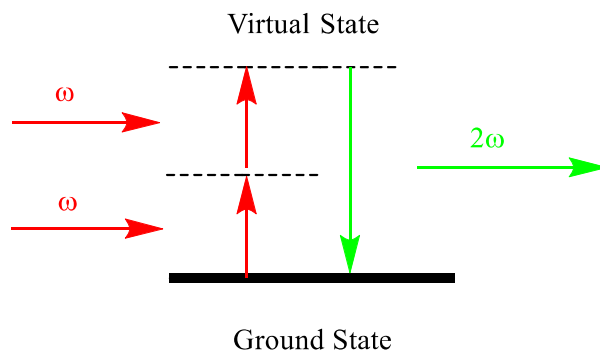


**Figure 1.2 Second Harmonic Generation**

Experimentalists can successfully direct synthetic techniques by combining chemical intuition with the knowledge gained from such cutting-edge simulations. It is not unexpected that there have been several thesis in the recent

literature presenting novel NLO response formalisms. With varied degrees of performance, several kinds of materials have been put forth as effective NLO materials. The range of compounds being studied by NLO has greatly increased during the past 20 years. Similar to this, significant work has been made in the field of quantum chemical techniques to compute the NLO properties of molecules, which has established several structure-property connections and given many invaluable insights into the ideal molecular structures. For instance, a number of polyphenylenes, polyenes, polynyas, their diphenyl-substituted equivalents, and compounds containing heterocyclic -systems have been used to monitor the effects of the  $\pi$ -conjugated system.<sup>[7]</sup>

SHG is the process of turning light with a certain frequency ( $\omega_1$ ) into light with a twofold frequency ( $\omega_2 = 2\omega_1$ ), or, put another way, the production of light with a wavelength ( $\lambda_2$ ) that is half that of ( $\lambda_1$ ) (shown in figure 2). Franken et al. made the initial observation of this phenomenon in 1961 and documented SHG in a quartz crystal stimulated by a ruby laser. There are 27 components in the third rank tensor known as the second-order NLO susceptibility. By considering the symmetry of the system, it is frequently possible to decrease this high number of tensor members. If a material has inversion symmetry.

In this case, inversion-symmetric materials are not SHG active within the electric dipole approximation, while higher order terms can still result in SHG, albeit weakly. Strong SHG response is possible in media where inversion is broken in a different way, such as the surfaces and interfaces of centrosymmetric materials or by the application of an electric field, or in systems that are not centrosymmetric (ferroelectric materials, piezoelectric crystals, chiral materials).<sup>[8]</sup>

The logical design and optimization of the crystal structure are essential since the optical characteristics of NLO materials depend on their crystal structures. The generally spherical cations contribute little, according to the anionic group theory, and the anionic groups govern the NLO characteristics and birefringence. As a

result, selecting the right anionic groups is crucial in producing NLO materials that are attractive. [9]

### 1.1.2.2 The Two-State Model:

The initial hyperpolarizability and molecular properties that may be utilized to assist design molecules as NLO compound are related by the two-state model of Oudar and Chemla<sup>[10][3]</sup>. When the examined molecule contains an absorption band near to the fundamental or second-harmonic (SH) wavelength, the initial hyperpolarizability can be resonantly amplified as a result of the amplification of higher excited states.

Because only one transition is assumed to be responsible for the NLO features, the static (off-resonance) initial hyperpolarizability  $\beta_0$  may be computed and is helpful for comparing the quadratic NLO qualities at various wavelengths.

$$\beta_0 = \frac{3\Delta\mu_{12}(\mu_{12})^2}{2(E_{max})^2} \quad (1.6)$$

Where  $\Delta\mu_{12}$  is the change in dipole moment between ground and excited state.  $\mu_{12}$  is the electronic transition dipole moment,  $E_{max}$  of the optical transition energy between ground and excited state.  $\beta_0$  is  $\beta$  extrapolated to zero frequency, by definition it does not vary with frequency ( $\beta$  does vary with frequency), which can cause major overestimation or underestimate of due to the participation of higher excited states, is measured under non-resonant circumstances when there is no reabsorption of SH. Equation (1.6) makes  $\beta_0$  increases when the energy  $E_{max}$  (the intramolecular charge-transfer) (ICT) decreases.

Where  $\lambda_{max}$  is the wavelength at maximum absorption and  $\lambda$  is the wavelength of the incident light (laser) that was used during the measurement. This model is only valid in the off-resonant regime, i.e., when the second-harmonic wavelength is much longer than  $\lambda_{max}$  (the wavelength at maximum absorption).

### 1.1.3 NLO Materials:

NLO materials recently offer a wide range of potential applications in cutting-edge optoelectronic and all-optical data processing technologies. Inorganic and organic NLO compounds make up the main two classes of NLO materials. On the other hand, hybrid organic-inorganic materials have recently attracted considerable attention due their enhanced properties and synergistic effects such as high and tuneable NLO properties.<sup>[11]</sup>

#### 1.1.3.1 Inorganic-Based NLO Materials:

The inorganic NLO materials are generally more stable than organic species. Numerous types of inorganic NLO materials, including inorganic salts, inorganic oxides, quantum dots, semiconductors, cluster compounds, etc., have been described for nearly 40 years.<sup>[12]</sup> However, compared to certain popular organic NLO compounds, inorganic NLO materials are unable to offer high photoelectric coefficient,<sup>[13]</sup> difficulties in alignment processing, and limitations in producing crystals. Therefore, many studies have focused on designing new materials with high NLO activity which has widely made from organic and organometallic compounds that contain electron donor and acceptor groups linked through a p-delocalized backbone (D- $\pi$ -A) model<sup>[14][15] [16]</sup>.

#### 1.1.3.2 Organic/Metallo-organic based NLO Materials:

The momentum of high-speed expansion cannot be ignored, and information-related technology innovation is getting more attention as broadband networks take over the world in the new age of information technology innovation and promotion. As more and more new application fields are developed, there is a growing demand to improve the underlying network infrastructure, speed up and increase the processing capability of massive data quantities. At the same time, the bandwidth of optical communication networks is being heavily taxed. One of the key elements of the design of optical communication networks is the electro-



optic modulator. Organic NLO materials have supplanted inorganic ones as the main components of modern electro-optical systems due to their high electro-optical coefficient, short reaction time, simple processing, and integration. Additionally, these materials have important uses in the biomedical, THz radiation, and high-speed communication industries.<sup>[17]</sup>

The capability of NLO materials to change the frequency of laser light interactions makes them some of the smartest materials available today<sup>[18]</sup>. Because NLO materials have so many uses in optoelectronics, photonics, and medicine, this field of study is still in its infancy.<sup>[19]</sup> Emerging technologies like imaging, photodynamic treatment, and sensing are always looking for novel, highly effective materials that are also affordable. The need for novel materials is always growing, and the one downside of using inorganic NLO crystals is that they are quite expensive. Recently, significant efforts have been made to investigate further NLO materials, including nanostructures, polymers, and molecular dyes.<sup>[19]</sup> Organic molecules stand out among them because of their significant NLO sensitivities, inexpensive production costs, and design flexibility. Due to their easy synthesis, purification, and relatively environmental friendliness, organic dyes have generated interest. Owing to their alluring NLO response, chemists have recently devoted close attention to organic molecules with electron donor (D) and acceptor (A) groups connected by  $\pi$ -conjugated bridges. By placing the right D, A units, and  $\pi$ -bridges in the right places, it is possible to finely tailor the intramolecular charge transfer (ICT) between the electron donor (D) and withdrawal group (A) and hence the NLO properties of D- $\pi$ -A compounds. Recently, such dipolar D- $\pi$ -A structures have displayed enormous hyperpolarizabilities.<sup>[14]</sup> Generally Higher values result from stronger electron donating strength and stronger electron withdrawing strength. As a result, the design and synthesis of NLO compound have made use of a variety of powerful electron donors and acceptors. Therefore, consideration should be given to the properties of the donor and acceptor subunits as well as joined length.

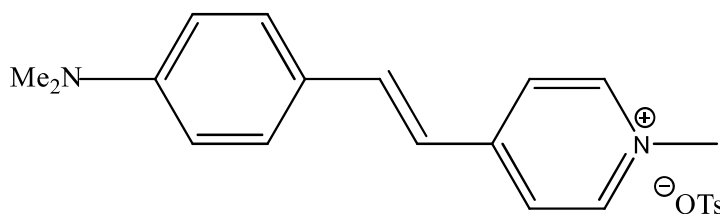
Organic NLO materials can provide flexible design, high photoelectric coefficients, low dielectric constants, and inexpensive production costs. Usually, the hyperpolarizability of the NLO compound is the source of the macroscopic NLO material properties. The primary basis for the optimization of organic NLO materials is frequently the design and modification of the D-A structure. The NLO compound must have substantial microscopic hyperpolarizability ( $\beta$  values) in order to realize practical utilization in device manufacture. It can also ensure that the conversion of microscopic data to macroscopic electro-optic (EO) coefficients is successful. Recent studies have mostly focused on two areas of compound design and synthesis:

- 1) to achieve high hyperpolarizability, extremely polar compounds are synthesized.
- 2) Enhancing the chemical structure to decrease the dipole-dipole interactions and boost the effectiveness of switching responses.

The concept of an "appropriate isolation group" and the site-isolation principle, which were introduced by Dalton et al.<sup>[20]</sup> and Zhen Li et. al.<sup>[21]</sup>, respectively, were effective ways to increase translation efficiency for high EO coefficients. By fine-tuning the electron donating and withdrawing strengths as well as optimizing the -bridge structure, Jindong Luo and Alex Jen et al. reported a number of high performances NLO compounds.<sup>[22][23]</sup>

Dimethylamino-N-methyl-4-stilbazolium tosylate (DAST) crystal (shown Scheme 1.1) is the only organic NLO compound utilized for commercial use as THz emitters, and available for spectroscopic uses due to its superior NLO capabilities and other advantages of being organic in nature. However, for a number of applications in the fields of astronomy, communication, testing, defence, and security, stronger THz radiation than that produced by DAST is required. The DAST molecule is composed of a positively charged stilbazolium compound and a non - polar tosylate anion. The stilbazolium compound is a dipolar compound with strong methyl pyridinium electron-acceptor and dimethyl

amino electron-donor groups (D- $\pi$ -A). This D- $\pi$ -A shape has a high initial hyperpolarizability ( $\beta$ ) and a low dielectric factor. In the instance of the DAST crystal, optical rectification or differential frequency techniques second order NLO processes are used to produce THz radiation. The physical phenomenon behind this mechanism is the DAST crystal's high initial hyperpolarizability ( $\beta$ ). [24]



**Scheme 1.1 Structure of Dimethylamino-N-methyl-4-stilbazolium tosylate (DAST)**

The comprehensive investigation of the NLO properties of organic complexes, which combine the characteristics of inorganic and organic complexes, has increased the scope to produce high performance NLO materials. Among them, organometallic complexes are advantageous for optical applications because the quantum efficiencies of singlet-triplet intersystem crossing a phosphorescence are greatly improved by linking the metal to the organic compound. As a result, an increasing number of researchers are examining how metals affect the characteristics of organometallic complexes to find the best possible candidates for NLO materials. [25]

Organic low-molecular NLO materials, high polymer NLO materials, metal organic complex NLO materials, etc. are some examples of the different organic low-molecular NLO materials that are currently being discovered or synthesized. Metal polyacetylene polymers, metal porphyrin organic complexes, metal phthalocyanine organic complexes, metal iridium organic complexes, metal carbonyl complexes, metal olefin organic complexes, and other compounds NLO materials are among them. The study of second-order NLO materials will

certainly focus on iridium (III) complexes in the future due to their superior performance, six-coordination, various valence states, and variety of coordination forms.<sup>[26]</sup>

First described was the second harmonic effect of metal organic compounds in 1986 by C. C. Frazier et. al. Since then, a number of metal organic compound non-linear effects have been identified. The metal-organic complex's NLO characteristics and color are directly influenced by its molecular structure. Metal-organic compounds have a variety of shapes due to the diversity of their ligand metals, which gives them an edge over NLO materials made of simple organic molecules. Metal atoms may create a variety of three-dimensional structures due to their diverse d or f electron numbers, oxidation states, and coordination numbers, which produce distinctive optoelectronic capabilities. For instance, the introduction of metal atoms can combine magnetic, electrical, and optical properties with optical properties to produce magneto-optical and electro-optical effects. The redox change of the central metal can also result in a chiral center, which can lead to a non-centrosymmetric crystal. Additionally, there are photons that transit from ligand to metal and from metal to ligand, and metal-organic complexes have more absorption bands, polarizability, and energy between the ground state and excited state than other types of complexes. The level difference is negligible, which helps the material's photoelectric response time. The growth of complicated research will be aided by the design and synthesis of ligands with unique structures. There have been several reviews of non-linear review papers including complexes of rhodium, zinc, and other metals. In contrast, there aren't many evaluations of iridium metal organic complexes.<sup>[27]</sup>

The importance of organic NLO materials in the creation of photonic platforms is amply supported by the available data.<sup>[28][29]</sup> Photonic applications have been greatly aided by the effective use of organic second-order NLO (or organic electro-optic, EO) polymers.<sup>[20][30]</sup> Plasmonic-organic hybrid (POH) modulators with organic EO materials take advantage of silicon photonics, organic

electrooptics, and plasmonic sub-wavelength light confinement while overcoming both the speed limitations of electronics and photonics of the efficient EO modulation of micrometer footprints.<sup>[31]</sup>

### 1.1.3.3 D- $\pi$ -A compounds:

Electronic charge would frequently be delocalized in NLO organo-based compound because to their-bond architecture. The initial hyperpolarizability ( $\beta$ ) is related to the intramolecular electrostatic interaction from the electron-donating moiety (D) through the attached spacer-linker to the electron-accepting moiety (A). In the literature, a number of framework types have been mentioned, including D-A, D- $\pi$ -A, D- $\pi$ - $\pi$ -A, D-A- $\pi$ -A, D-D- $\pi$ -A, D- $\pi$ -A- $\pi$ -D, and A- $\pi$ -D- $\pi$ -A.<sup>[32][33]</sup> The literature is rife with a vast diversity of -linkers, and the nature of both D and A moieties play a crucial part in creating a successful NLO response. For developing A-D- $\pi$ - $\pi$ - $\pi$ -A and D-A-D- $\pi$ - $\pi$ -A organic molecules, by using suitable D,  $\pi$ -conjugation spacers and A, a push-pull layout has been created.<sup>[34]</sup> These push-pull designs increase the NLO response by reducing charge recombination, increasing the asymmetric electronic distribution, relatively decreasing the HOMO-LUMO energy gap, increasing the transition range at longer wavelengths, and affecting charge transition. According to the literature, long-conjugated structures are the best types of materials for NLO. The creation of high performance NLO materials has since been approached in a variety of ways, including the electron push-pull mechanism, extended electron conjugated systems, synthesis of octupolar molecules, and altering the quantity and location of metals in different complexes. The incorporation of extra electrons into a system causes an increase in hyperpolarizability, which in turn affects the NLO properties, and is a relatively novel technique for improving the NLO responsiveness of materials. According to earlier studies,<sup>[35]</sup> the system with extra electrons might provide guidance for fresh design ideas for unique NLO materials. In this context, advanced NLO materials are emphasized as electrised

and alkalides with extra electrons. Alkali metal atom adsorption on various nanostructures is a useful method for obtaining extra electrons in a system. Numerous NLO materials are created in this area through both theoretical and experimental design.<sup>[36]</sup>

#### **1.1.4 NLO Switchable:**

Due to their wide range of applications, including in optical computing, optical data transmission, and electro-optical devices<sup>[37]</sup>, a number of second-order organic NLO materials have been the subject of extensive experimental and theoretical research during the past twenty years. Organic NLO materials have a quicker response time, greater thermal stability, a better optical frequency transform, and a stronger intramolecular charge transfer than inorganic NLO materials. Furthermore, organic NLO materials have the ability to flip between two stable states reversibly, which is typically accompanied with switchable "ON" and "OFF" NLO behaviour. These materials switchable behaviour, which is often brought on by oxidation/reduction processes<sup>[38]</sup>, pH changes<sup>[39]</sup>, light, and temperature variations, is a key feature for their use.<sup>[24]</sup> Due to the promise of switchable NLO materials in optical device applications. Several investigations on finding new switchable NLO materials have been conducted during the last two decades.<sup>[40][41]</sup> Finding new materials with remarkable nonlinearities with the switching ability is necessary.

#### **1.2 Polyoxometalates (POMs):**

Since the first functioning laser was discovered, NLO materials have attracted a lot of attention. NLO materials are now being used in several cutting-edge high-tech applications, such as laser shows, telecommunications, optical data writing, and SHG spectroscopy. Only few types of materials with high and efficient NLO response are present. Every class of material has certain inherent benefits and disadvantages when it comes to real-world applications. However, the organic

and organometallic classes of molecules have consistently been at the forefront of NLO material science design. Organic molecules have a wide range of functional groups that may be used to create a number of unique NLO materials.<sup>[42]</sup> One of the main objectives of molecular electronics has been to use individual molecules as potential units in nanotechnology (moletronic). One of the most crucial worldwide challenges to address, as the size of future electronic systems shrinks to nano- and sub-nanometre (molecular) levels, is the creation of high-performance and thermally stable molecular components (such as resistors, rectifiers, or memory). Among NLO materials, organic and organometallic compounds that contain electron donor and acceptor groups linked through a  $p$ -delocalized backbone (D- $\pi$ -A) are of major interest in designing such molecular NLO materials. However, transparency/non-linearity trade-off issues are the main challenges limiting the NLO enhancement of both organic and metallo-organic materials.

On the other hand, inorganic compounds known as POMs have drawn a lot of interest because to their distinctive features and wide range of uses, including energy conversion (electrochemical cell), capacitors, memory, and catalytic magnets. Since 1998, they have been explored as potential electronics materials. Recently, substantial experimental research has been done on the electron-transport characteristics of films made using POM and their prospective application in memory or other types of electronic devices.<sup>[43][44]</sup> Redox behaviour, which is defined by accepting one or more electrons while experiencing no structural changes, is a special characteristic of many POMs. POMs made from organic materials have attracted a lot of interest because of their distinctive architecture and possible uses. The properties of both the POM cluster and organic part are expected to be combined and enhanced in these hybrid systems with potential synergic effects. In general, POMs have three types, heteropolyanions, isopolyanions, and giant nanosized polymolybdate clusters, which are shown in (figure 1.3).

Only one kind of high-valent group 5 or group 6 transition metal ion may be found in isopolyanions. More than 30 isopolyanions have been identified so far, with the Lindqvist and octamolybdate being the most extensively researched. The Klemperer and co-workers' synthetic approach may be used to create the Lindqvist structure, hexamolybdate ion  $[\text{Mo}_6\text{O}_{19}]^{2-}$ , which has high thermal and chemical stability.<sup>[45]</sup> Six edge-shared  $\text{MoO}_6$  octahedra are arranged in a compact configuration to make up its structure. Octahedral symmetry characterizes the whole structure. These intriguing qualities, such as their redox characteristics and capacity to take one electron, make them promising building blocks. (electron-relay).<sup>[46][47][48]</sup>

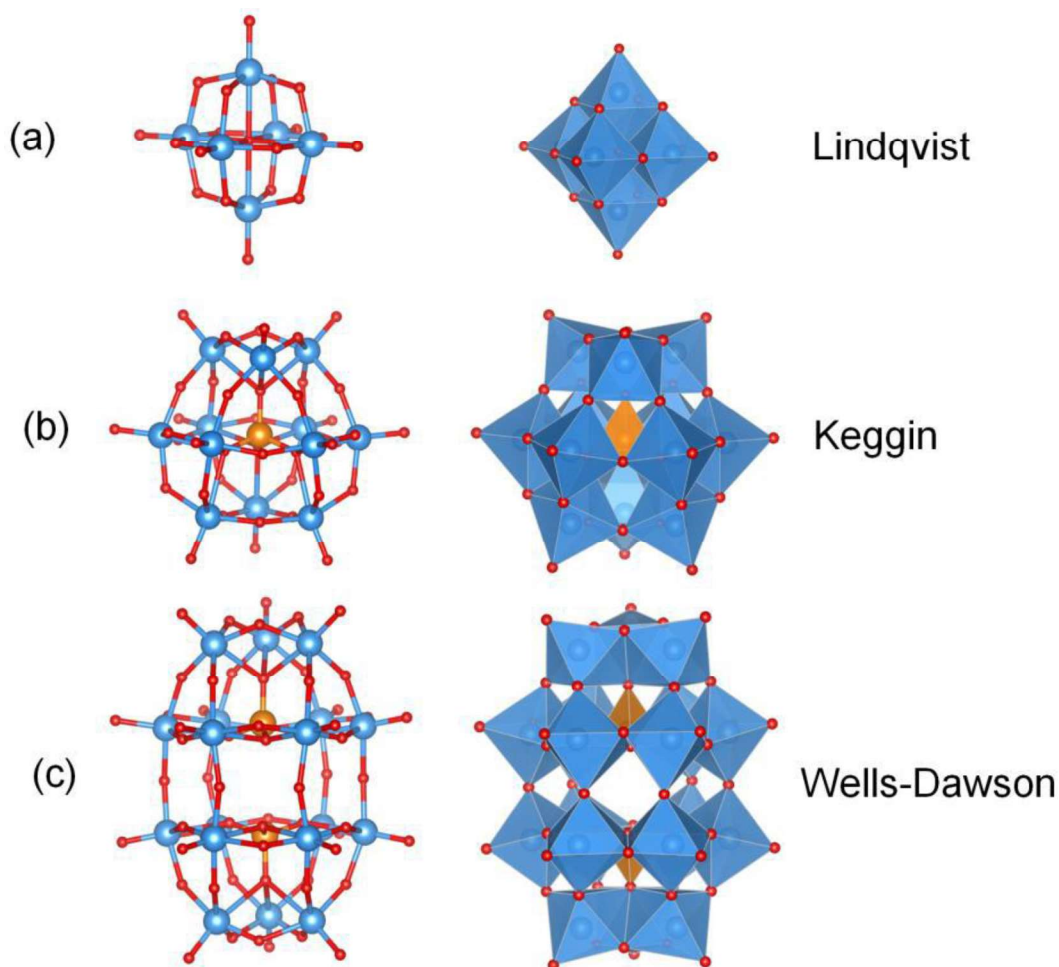




Figure 1.3 Ball-stick and polyhedral representations for three most common polyoxometalate structures. (a) Lindqvist anion:  $[M_6O_{19}]_x^-$ ; (b)  $[\alpha-\{XO_4\}M_{12}O_{36}]_y^-$ : Keggin anion; (c)  $[\alpha-\{XO_4\}_2M_{18}O_{54}]_z^-$ : Wells-Dawson structure.<sup>[49]</sup>

### 1.2.1 Lindqvist-Organoimido Derivatives:

Among the various organic derivatives of POMs, the organoimido derivatives POMs coupled with small organic functional groups are considered to be the fundamental building block for more sophisticated and durable POM-organic hybrid materials. There are several methods to functionalize POMs that create organoimido derivatives of POMs.<sup>[50]</sup> Hexamolybdate ion has received the greatest attention from researchers studying the organoimido-POM derivatives in recent years,  $[Mo_6O_{19}]^{2-}$ .<sup>[51]</sup> Ingvar Lindqvist, a Swedish chemist, published the Lindqvist for the first time in 1950. It has the general formula and it is the smallest and simplest of the conventional POMs  $[Mo_6O_{19}]^{2-}$ . The hexamolybdate ion,  $[Mo_6O_{19}]^{2-}$ , one of the most well-known POM clusters due to its thermal and chemical stability and simplicity of preparation, which possesses the so-called Lindqvist structure. A core oxide ion is surrounded by an octahedral cage made up of six metal and eighteen oxygen atoms in the Lindqvist structure. The octahedral environment encompasses each of the six metal atoms. They each coordinate three times to one terminal oxygen atom in addition to the central oxygen atom, producing a terminal metal-oxo group (MO), and share four more doubly bridging oxygen atoms ( $\mu$  2-O atoms) with neighboring metal atoms. These molybdic groups (MoO) for the hexamolybdate are sufficiently reactive for the terminal oxygen atoms to be directly substituted by a variety of nitrogenous species, such as di azenido, diazoalkyl, and imido groups.

The Lindqvist hexamolybdate organoimido derivatives have drawn a lot of interest among these organic-inorganic hybrid systems. Due to their high interactions between d-p orbitals and p-p electrons, these species have exceptional optical, catalytic, electrical, and magnetic capabilities. Being a novel unit, it can create a variety of intricate hybrids due to their easy of processing. In

addition, their molecular structure is comparable to nanoscale metal oxides, which are more suited for device applications. Huge current densities are anticipated to flow through these molecular clusters even at low bias voltage circumstances, showing that the POM is more promoted than the organic species. Organoimido derivatives are among the many classes of chemically functionalized POMs and are of special interest. In addition to the imido metal-nitrogen linkage's extraordinary durability, which allows for additional structural change of the organic component that is anchored to the cluster, delocalization of the organic p electrons on the POM cluster may result in a new category of electronic hybrid materials.<sup>[52]</sup> Because the organic electrons may extend their conjugation to cluster d electrons, resulting in strong d- interactions, the organoimido derivatives of Lindqvist-type hexamolybdate,  $[\text{Mo}_6\text{O}_{19}]^{2-}$ , have drawn special interest. POMs of the Lindqvist hexamolybdate type have many organoimido derivatives that have been reported.<sup>[50]</sup> Basically, different organoimido ligands might replace one or possibly all six terminal oxo groups of a hexamolybdate ion. With a variety of imido releasing reagents, the terminally substituted mono- and even multi-functionalized organoimido derivatives of POMs have been created.<sup>[53]</sup> Matta et. al. direct functionalization of the POM cluster of hexamolybdates few years ago made it easier to carry out the subsequent functionalization of POM cages.<sup>[54]</sup> A novel and very effective method for the selective synthesis of difunctionalized organoimido hexamolybdate derivatives was investigated by Xu et. al.<sup>[55]</sup> Organoimido derivatives of POMs may be useful for creating covalently tailored POM-based hybrid composites, according to research by Lu et. al.<sup>[56]</sup> These hybrids are intriguing electrically effective materials due to the strong electronic interactions between unsaturated organic chains and POM clusters (hexamolybdates) in them. POMs have an electro-active nature, therefore when combined with electrically active organic groups, they provide materials with a variety of potential applications in sensors, solar energy conversion, molecular device processes, and

biological materials.<sup>[57]</sup> The excellent work of Matta,<sup>[54]</sup> Proust,<sup>[58]</sup> and Errington et. al.<sup>[59]</sup> has led to the development of three different types of reactions for the synthesis of imido derivatives of the hexamolybdate. As memorialising reagents, they include reactions with phosphamides, isocyanates, and aromatic amines. The hexamolybdate cluster's six terminal oxygen atoms (and occasionally some bridging oxygen atoms) can be entirely replaced with organoimido ligands using these techniques. Hexamolybdate's mono-, di-, and multi substituted organoimido derivatives have been synthesized and structurally described recently.<sup>[60]</sup>

### 1.2.2 Organoimido-Lindqvist as NLO Materials - Literature Servay:

Since POMs are good electron acceptors and hence could be used with organic donors to create D- $\pi$ -A compounds and, they have emerged as new, potential NLO materials. There have been several charge-transfer salts created. These sorts of salt are always formed when organic and organometallic cations are combined with POM anions. However, the relatively weak organic and inorganic interactions that these charge transfer salts provide in the solid state have precluded an efficient electron transfer between the two components. to create effective online communication.<sup>[61][62]</sup> As a rare chance to explore at the molecular level the reactivity of isolated heterometal sites embedded inside a matrix of another metal oxide, heterometallic POMs are of special interest because they help to build a foundation for understanding the function of mixed oxide catalysts.<sup>[63]</sup> Only a small number of NLO-active materials include POM anions, and they all focused on the second-order NLO response. However, recent theoretical and experimental investigations have demonstrated that chiral POM-based materials exhibit outstanding NLO responsiveness.<sup>[64]</sup>

Organoimido derivatives of POMs (especially ones of the Lindqvist type) are regarded as excellent NLO crystals due to their strong D-synergistic effect between both the delocalized electrons of the organic moiety and the vacant p-d orbitals of the POM group, strong electronic transitions, versatility due to a wide

range of metals, and ease of modification to set the stage for desired applications. Since Yang Likai and her colleagues' ground-breaking study, additional research has been done that initially assessed the NLO response of organoimido substituted hexamolybdates based on various organic-inorganic hybrid systems in order to better understand the NLO reaction of POM-based hybrid materials.<sup>[62][65]</sup> The NLO features of this kind of material have received a lot of attention in recent scientific research. In these hybrid organic-inorganic materials, the lengthening of  $\pi$ -conjugation or switching from a single ring to a double ring result in a change in the direction of charge transfer, which can enhance the second-order NLO response compared to crystals that are entirely inorganic or pure organic compounds.<sup>[24]</sup>

Because of their strong d-d interactions between the organic delocalized electrons and the cluster empty d orbitals, intense electronic transitions, versatility via a wide range of metals, and simplicity of modification to produce building blocks for specific applications (noncentral symmetric molecules), POM-based organic and inorganic hybrid materials, especially organoimido-Lindqvist derivatives, are excellent candidates as NLO materials.<sup>[52][66][67][68]</sup> However, only calculations based on large second-order NLO coefficients have been used to address their optical characteristics up to now.<sup>[69][64]</sup> Such materials are an appealing target for usage as redox switchable NLO compounds as a result of this prediction and the well-defined, rapid electrochemistry of the Lindqvist anion.

Recently, AlYasari et. al. reported the first experimental second-order NLO activity using the HRS method, as well as the two-photon absorption (experimentally and theoretically) activity for donor-functionalized arylimido-POMs. The studied systems showed strong electronic connections (and hence strong charge transfer transitions) between the organic moieties and POM clusters, resulting in strong NLO responses with much improved transparency/non-linearity trade-offs to comparable organic systems.<sup>[70][71]</sup> Moreover, the results showed that the NLO responses are generally higher than

those obtained from comparable structures with organic acceptors. Recently, Champagne and co-workers performed DFT calculations of the first hyperpolarizability  $\beta$ -values for these derivatives and compared them with experimentally derived ones.<sup>[72][73]</sup> The results revealed good agreement between the experimental and calculated values demonstrating the validity of the model used to compute  $\beta$ -values. These results have motivated us to further investigate the design of POM-based NLO compounds with substantial NLO responses.

### 1.3 Julolidine-Based Donors:

One of the groups of fluorescent dyes that has received the greatest research attention is the julolidine derivatives, which are also likely one of the fluorescent chemicals that are employed the most. Julolidine derivatives have been demonstrated to offer potential in a wide range of applications, including NLO materials, dye-sensitized solar cells, antidepressants, tranquilizers, and photoconductive materials.<sup>[74]</sup>

The family of N-heterocyclic aromatic compounds known as julolidine has drawn the attention of several different research groups.<sup>[75][76]</sup> 2,3,6,7-tetrahydro-1H,5H-benzo[i,j]-quinolizine is the most basic julolidine. This chemical derives structurally from aniline and forms a fused three six membered ring structure with two alkyl substituents in the ortho position sharing a nitrogen atom, as shown in (figure 1.4).

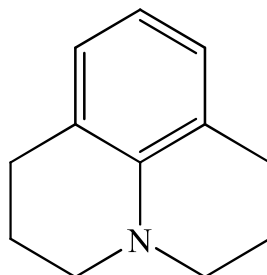


**Figure 1.4 Structure of Julolidine(2,3,6,7-tetrahydro-1H,5H-benzo-quinolizine)**

Julolidine has been explored for their potential as fluorescent probes for a variety of applications due to their fluorescent characteristics. Additionally, due to their

high energy conversion efficiency, these compounds may be used to create solar cells. As fluorescence-based sensors, julolidine may also be used to assess the stability of protein aggregation in medicinal formulations. Additionally, certain julolidines with altered structural properties have demonstrated highly potential bio-medical applications. Examples include using julolidines as blood viscosity measuring probes, photoinduced neurotransmitter amino acid release, and bio-image sensors (e.g., DNA, RNA, lysosome, and mitochondrial pictures).<sup>[77][78]</sup>

Modified julolidine derivatives were discovered to be one of the most effective electronic donors for NLO compounds.<sup>[79][80]</sup> To attain high EO coefficients, a number of Julolidine-based NLO compounds have been developed, synthesized, and had their structural features altered. The inappropriate integration of strong donors and acceptors, such as the acceptor CF<sub>3</sub>-Ph-TCF, was discovered to be ineffective for achieving high EO performance. Finding the structure-property link and offering a design rule for julolidine-based NLO compounds are important. In order to examine the intricate structure-property interactions, we easily synthesized four julolidine-based NLO compounds with various donors and acceptors.<sup>[81]</sup>

Due to their excellent chemical stability, thermal stability, and low toxicity, julolidine derivatives are frequently employed in electroluminescent devices.<sup>[82]</sup>

In the solid state or in concentrated solutions, julolidine improves solubility and avoids concentration quenching. When combined with dicyanomethylpyran modules, julolidine-based materials have been employed as red emitters in OLEDs and in push-pull systems for low-energy exciplex emission in the past.<sup>[83]</sup>

It has been observed that fluorescent molecules called fluorescent molecular rotors (FMRs) go through non-radiative relaxation from the fluorescent excited state. FMRs are fluorescent molecules made up of an electron donor unit conjugated with an electron acceptor moiety. Although julolidine FMRs are often used as viscosity sensors, it is still unclear how they behave in polymer matrices. Examples of how to gauge free volume and plasticity in thermoplastic polymers

as well as how to determine the molecular weight dependence of viscosity in polymer melts have been documented.<sup>[84]</sup>

The fused julolidine moiety's high electron-donating capacity and confined mobility are very useful at enhancing the photophysical characteristics. Consider the positive photophysical properties that julolidine-fused fluorophores often exhibit, such as their high quantum yield, their red-shifted emission and absorption, and their strong photostability. Julolidine derivatives have recently seen significant use in a wide range of fields, including sensing, imaging, and NLO materials. Due to its large  $\pi$ -conjugated system and potential electron donating capability, many julolidine dyes have been employed in dye-sensitive solar cells.<sup>[85]</sup> Due to their excellent capacity to donate, julolidine and its derivatives recently attracted a lot of interest. A number of fresh compounds based on these groups do indeed exhibit strong EO performance. Although these novel donor groups have potential uses, their advancement in improving EO responsiveness has received very little attention.<sup>[86]</sup>

**1.4 Aims of Study:**

The primary goals of this research project are to investigate the NLO characteristics of POM complexes based on julolidine derivatives and to create novel compounds by structurally altering julolidine groups following steps below:

1. The research will focus on designing and studying by using means of quantum chemistry (DFT) new hybrid materials based on POMs functionalized with strong donors such as julolidine donor groups and its derivatives, as switchable NLO compounds.
2. Improving the electro-optical and hence the NLO properties for the System under study.
3. Studying effect of methylation ortho to the imido-groups on the stability of the derivatives and hence the ability of switching NLO properties.
4. Studying effects of phenyl, alkyl, and other substitution groups on the julolidine structure that effects their donor ability and hence tuning the ligand-to-POM-charge transfer.



# **Chapter Two**

## **Computational Theory and Methods**

## Chapter Two

## Computational Theory and Method

**2.1 Schrödinger Equation:**

The initial step in the study of quantum chemistry was made possible by the discovery of Schrödinger's wave equation in 1926.<sup>[87]</sup> The Schrödinger equation defines how a physical system's wave function behaves over time. The Schrödinger equation may be used to analyze the distribution of electrons within a molecule:

$$\hat{H} \Psi = E \Psi \quad (2.1)$$

Where  $\hat{H}$  is the Hamiltonian operator that acts upon the wave function ( $\Psi$ ) to give the energy, an electron's spatial location is described by the wave function, while the system's overall energy is represented by the Hamiltonian operator. Schrödinger's equation has precise solutions, but finding them in multi-electron systems is nearly difficult since the complexity of the computations increases exponentially with the number of electrons in the system.<sup>[88]</sup> When there are several electrons, the equation becomes a three-body issue where the nucleus must be factored in. These many-body problems can't be precisely solved mathematically; hence approximations are needed. The Born-Oppenheimer approximation can be used to solve the multi-electron time-independent Schrödinger equation.<sup>[89]</sup> This is predicated on the idea that since nuclei are far heavier than electrons, their relative motion may be separated since the nucleus is practically motionless in relation to the electrons. This enables the electronic and nuclear components of the Schrödinger equation to be solved independently. Ab initio approaches, semi-empirical methods, and DFT are some additional approximations that may be used to reduce the complexity of the Schrödinger equation. The Latin phrase "ab initio" means "from the beginning." When computing using the ab initio procedures in quantum chemistry, variables are parameterized directly from theoretical notions rather than through the use of

experimental data. These methods have been widely used in the last three decades to study molecules. To ascertain the electronic energies and wave functions of atoms, molecules, and all other chemical species is the goal of the field of computational quantum chemistry. Although one usually has to start with a realistic beginning structure of the molecule when completing a computation, the molecule is assumed to be a collection of positive nuclei and negative electrons sensitive to Coulombic potentials in order to solve the Schrödinger equation from first principles. It is inevitable that approximations will be made to streamline computations when attempting to apply ab initio techniques to complicated systems.<sup>[90]</sup>

Ab initio and semi-empirical approaches are the two main divisions of electronic structure techniques. Ab initio computations are those that are generated from theoretical concepts without the use of experimental data, whereas semi-empirical computations use experimental data to parameterize their procedures. Better outcomes are possible with higher quality approaches, but the computing cost increases exponentially with the number of atoms. Several well-known ab initio techniques with the corresponding scaling factor ( $N^n$ ), where  $N$  is the quantity of basis functions employed, scaling exponentially by  $m$  and affects the computing expense of the technique being applied Configuration interaction (CI), coupled cluster (CC), HF ( $N$ ), and many body perturbation theory (MBPT) ( $N$ ). The more complicated of these techniques is therefore only practical for molecules with 20 or fewer atoms. The correlation term requires the computation of multi-determinate wavefunctions as opposed to a single Slater determinant, which increases the computational expense. When calculating big systems, which are typical of organometallic systems, a trade-off, between speed and accuracy must be made while making sure the appropriate degree of theory is used for the chemical challenge at hand. Additionally, quicker electronic structure simulations are preferred when examining a range of isomers and potential catalytic routes. Compared to the wavefunction-based approaches previously outlined, DFT is the

most popular method since it represents the electron density as a function of the ground state geometry.

## 2.2 Quantum Chemistry:

Computers have recently developed to the point that investigations of chemical systems resolved to the level of the electronic structure are possible. These approaches use a Hamiltonian to use quantum chemistry (QC) methods to calculate the system's energy and the forces that are operating on its atoms. A spectrum of levels of theory based on Hamiltonian parameterization may be used to categorize QC, with ab initio approaches having almost little parameterization and semi-empirical and empirical methods introducing parameters in an effort to decrease computing effort.

Molecular dynamics and quantum chemistry techniques have been used to provide light weight on slip processes in dynamical settings utilizing model systems that are resolved to the level of the electronic structure. These models are capable of capturing bonding alterations that may be attributed to friction, wear, and tribo-chemical processes. These techniques can only study tiny systems at most a few hundred atoms over a short period of time (a few hundred picoseconds at most).<sup>[91]</sup>

The result, or the precise value observed, depends in part on the quantum state of a quantum item, such as an atom, proton, or electron, when a measurement is made of it. The description of an object's attributes, such as location, energy, spin, etc., as they actually exist, is called its state. An electron, for instance, can spin either clockwise (referred to as "spin down") or counter clockwise (referred to as "spin up"). Operators that act on the state allow for the manipulation or measurement of states. The state is an eigenstate of that operator when it extracts information from a state, such as the electron's spin, without affecting the state of the object. The information is a scalar known as the eigenvalue.<sup>[92]</sup>

### 2.3 Hartree-Fock Self Consistent Field:

A clever trick to come to approximate solutions of Schrödinger equation (differential equation), called the HF method, is to take Eq. 2.1 and add/subtract a constant term:

$$\hat{H} = -\sum_{i=1}^n \frac{1}{2} \nabla_i^2 - \sum_{i=1}^n \sum_{A=1}^N \frac{Z_A}{r_{iA}} + \sum_{i=1}^n V_{ri} + \underbrace{\sum_{i=1}^n \left( \sum_{j>i}^n \frac{1}{r_{ij}} - V_{ri} \right)} \quad (2.2)$$

The physical reasoning behind it is the following: with a carefully selected potential  $V(r_i)$  the term  $H_{pert}$  may become sufficiently small so that it can be neglected, although neither  $\sum_{j>i} \frac{1}{r_{ij}}$  nor  $\sum_{i=1}^n V(r_i)$  are separately small. When the function  $V(r_i)$  has been determined, the Hamiltonian will be a sum of one-particle terms:

$$\hat{H} = \sum_{i=1}^n \hat{F}(i) \quad (2.3)$$

Where

$$\hat{F}(i) = -\frac{1}{2} \nabla_i^2 - \sum_{A=1}^N \frac{Z_A}{r_{iA}} + V(r_i) \quad (2.4)$$

Now the variables of the electrons are separated, the solution is obvious:  $\Psi(r_1 \dots r_i)$  will be the product of the solutions of the one-electron eigenvalue equations  $\hat{F}(i)\phi_k(i) = \epsilon_k \phi_k(i)$ . The potential energy operator,  $V(r_i)$ , represents the averaged, repulsive energy that electron  $i$  feels, due to the presence of all other electrons. Electron  $i$  moves in the mean field created by all other electrons, an effective potential so to speak. By ‘replacing’ the inter-electronic repulsion term with a simple sum of one electron operators  $V(r_i)$ , the electrons can be treated as being separate and independent of each other. It is important to stress that this independent-electron model is an approximation of reality, and the approximations are actually so severe, that quantitative results are rarely correct.

### 2.4 Electron Correlation:

The approximations used in the HF method's development are to back to for the discrepancy between the HF limit and the real energy. It is not accurate to think of all electrons as autonomous entities, each traveling in their "own" averaged potential. If, for instance, electron 1 occupies a patch of space at point  $r_1$ , it is extremely unlikely that any electron 2 will be present nearby. Greater than in the mean field approximation, electrons avoid one another. As a result, the predicted energy is excessively high; lowering it by accounting for electron correlation. What percentage of the system's overall energy is this correlation energy, according to the question? It's surprisingly fairly low. The remaining 1% of the entire energy in a helium atom, for instance, is correlation energy since the HF limit catches 99% of the total energy compared to the real energy<sup>[93]</sup>. This 1% is nevertheless essential for chemical precision since, in the case of helium, this 1% correlation energy is already equal to 26 kcal/mol. Breaking chemical bonds and computing Gibbs free energies of formation normally demands an accuracy of the order of several kcal/mol. However, in fact, it is typically not so terrible because the inaccuracy created when comparing different energies is of a considerably lesser scale. However, electron correlation is significant and must be taken into consideration in order to reach quantitative conclusions.

### 2.5 Density Functional Theory (DFT):

DFT is a quantum mechanical technique frequently used in computations involving the gas phase and solid states for examining the electronic structure of many-body systems. In contrast to wavefunction-based techniques, functionals that is, functions of another function of the spatially dependent electron density are used to derive the features of a many-electron system. Due to the fact that the electron density is seen as a single-body issue and that the number of variables remains constant, DFT approach is computationally efficient. Compared to many-body wavefunction approaches, where each electron contributes three variables,

DFT is a lot easier. As a result, DFT is frequently preferred for designing catalysts over ab initio calculations since it has a lower computing cost while keeping a similar level of precision.<sup>[94]</sup>

The total energy of an electronic structure calculation is expressed as a functional ( $E[\rho]$ ) of the electron density ( $\rho$ ) that takes the general form:

$$E[\rho] = T_s[\rho] + \int dr v_{ext}(r)\rho(r) + V_H[\rho] + E_{xc}[\rho] \quad (2.5)$$

The first term,  $T_s$ , represents the Kohn-Sham electronic kinetic energy approximation. The next term,  $v_{ext}$ , represents the external potential of coulombic interactions between the nuclei and electrons and is expressed in spherical coordinates ( $r$ ). The third term,  $V_H$ , is the Hartree or Coulomb energy for the repulsion between the electron density and itself. The fourth term,  $E_{xc}$ , is the exchange-correlation functional, which accounts for electron-electron interactions.

Scientists can find materials with desirable properties in vast data repositories by using high-throughput computational materials design, creating novel compounds with necessary properties via crystal structure prediction, or learning directly from data thanks to the rapid increase in computational power of current supercomputer architectures and significant advances in first principles calculations. Finding the structural components, referred to as functional modules (FMs), that govern a compound's attributes during the screening or prediction process is crucial for success in both organic and inorganic compounds. Novel materials may be easily designed, predicted, and synthesized with a solid understanding of FMs.<sup>[95]</sup>

In physics, chemistry and materials science, DFT are a computational quantum mechanical modelling technique used to look into the electronic structure (or nuclear structure) of many-body systems, such as atoms, molecules, and condensed phases. After decades of development, improvement in methodology

and implementations have reached a point where predicted properties, like lattice constants, cohesive/adsorption energies, band structures, surface reactivity, thermochemistry, rate constants, and other physical and chemical properties, can be obtained with reasonable to high quality. As a result, it is possible to analyze the microscopic mechanism by building interaction models of the various components, and a number of necessary parameters can be calculated without compromising the integrity of the system. This greatly complements experimental studies and even ventures confidently into areas that have not been explored experimentally. [96]

DFT is now a crucial method for simulating the characteristics of molecules and materials. Therefore, it looks tempting to apply DFT for NLO property prediction as well. DFT, which has been shown to be an effective tool to study the characteristics of POMs, is being used by our lab to investigate first and second hyperpolarizability of POMs and their derivatives. [97]

The results of the POM DFT investigations have improved. By using DFT, we have examined the electrical characteristics, bonding nature, and stability of POMs. The creation of novel, intriguing POM-based molecular NLO materials as well as the justification of the observed features of the POM system in itself might benefit from theoretical investigations of NLO properties. In this thesis, we used DFT simulations to anticipate the NLO characteristics of hexamolybdate organoimido derivatives and to show how these POMs got their NLO features. The goal of the current work is to take a preliminary step toward a deeper comprehension of the NLO characteristics of POMs. [61]

The structural characteristics of the ground and excited states, as well as the vibrational frequencies and energies of molecules of the D- $\pi$ -A type, have all been extensively described by DFT over the past ten years. Additionally, the computed values acquired using this approach are accurate and efficient in terms of evaluating a variety of molecular attributes. The DFT is employed in the



theoretical modelling of drug creation as well as the search for novel materials used in photonics.<sup>[98]</sup>

Our team used DFT to compute a number of hexamolybdate complexes, and the findings demonstrate that the charge transfer from organoimido to hexamolybdates helped to improve the NLO responses of one-dimensional organoimido derivatives of hexamolybdates. However, by adjusting the length of an organic ligand, one may change the direction of charge transfer. The design of the novel NLO materials will benefit from an understanding of the structure-property connection with organoimido POM derivatives. This research could help in the development of high-performance NLO materials.

### 2.5.1 Time-Dependent Density Functional Theory (TDDFT):

The study of exciton transfer and charge-recombination processes in organic electronic devices is aided by the time dependent extension of DFT (TDDFT), which enables the computation and interpretation of optical absorption and emission spectra.<sup>[99]</sup>

Correlated electron motion plays a significant role in the spectra described in the previous chapters. Further, placing an atom, molecule or solid in a strong laser field reveals fascinating non-perturbative phenomena, such as non-sequential multipleionization, whose origins lie in the subtle ways electrons interact with each other. The direct approach to treat these problems is to solve the (non-relativistic) time-dependent Schrödinger equation for the many-electron wavefunction  $\Psi(t)$ :

$$\hat{H}_{(t)}\Psi_{(t)}=i \frac{\partial\Psi(t)}{\partial t}, \hat{H}_{(t)}=\hat{T}+\hat{V}_{ee}+\hat{V}_{ext(t)} \quad (2.6)$$

for a given initial wavefunction  $\Psi(0)$ . Here, the kinetic energy and electron-electron repulsion, are, respectively:

$$\hat{T} = -\frac{1}{2} \sum_{i=1}^n \nabla_i^2 \quad \text{and} \quad \hat{V}_{ee} = \frac{1}{2} \sum_{i \neq j}^n \frac{1}{|r_i - r_j|} \quad (2.7)$$

and the “external potential” represents the potential the electrons experience due to the nuclear attraction and due to any field applied to the system (e.g laser):

$$\hat{V}_{\text{ext}(t)} = \sum_{I=1}^N v_{\text{ext}}(\mathbf{r}_i, t) \quad (2.8)$$

For example,  $v_{\text{ext}}(\mathbf{r}_i, t)$  can represent the Coulomb interaction of the electrons with a set of nuclei, possibly moving along some classical path,

$$v_{\text{ext}}(\mathbf{r}_i, t) = \sum_{v=1}^{Nn} \frac{Z_v}{|r - R_v(t)|} \quad (2.9)$$

where  $Z_v$  and  $R_v$  denote the charge and position of the nucleus  $v$ , and  $Nn$  stands for the total number of nuclei in the system.<sup>[100]</sup>

The hybrid TDDFT excitation energies are generally excellent for valence excitations; nevertheless, the findings are usually in question for some problematic circumstances, such as Rydberg and charge transfer (CT) states, or  $\pi \rightarrow \pi^*$  excitations of conjugated systems. Only one family of the aforementioned transitions may be reasonably predicted by a particular hybrid functional; nonetheless, additional research is needed for their widespread use. Numerous strategies were devised to enhance the outcomes for both the ground- and excited-state characteristics. The range separated (RS) and double hybrid (DH) hypotheses are the two most notable.<sup>[101]</sup>

Today, TDDFT which balances computational accuracy and efficiency, has emerged as one of the most potent techniques for probing electronic structure and optical excitations. To calculate the excitation energy, ionic force, and nonadiabatic coupling of excited states in molecular- and solid-state materials in particular, linear-response TDDFT has been frequently used.<sup>[102]</sup>

### 2.5.2 $\omega$ B97XD:

Recently, a methodical optimization process was used to increase the overall accuracy that the LC functionals can achieve. One significant finding is that, for all attributes employing the LC form, optimizing LC and hybrid functionals with the same number of parameters in their GGA exchange and correlation terms yields considerably superior results. The LC functional that results is known as  $\omega$ B97XD.<sup>[103]</sup> Re-optimizing the entire functional with one more parameter, which defines the  $\omega$ B97XD functional and corresponds to an adjustable proportion of short-range exact exchange, leads to further statistically significant improvement. These results are supported by independent test sets that span thermochemistry and non-covalent interactions. However, issues like the absence of dispersion interactions (London forces), which are related to the correlation hole's lack of non-locality, continue to exist since semi-local correlation functionals cannot account for long-range correlation effects.<sup>[104]</sup> In this thesis,  $\omega$ B97XD functional was chosen for long-range correlation effects of the NLO effects for hexamolybdate organoimido derivatives, which has been previously tested and applied by Rtib *et al.*<sup>[72]</sup>

### 2.6 Basis Sets:

An important consideration in any quantum calculation is the choice of basis set. Mathematically, a basis is a complete set of linearly independent vectors which together in linear combination, can represent any possible vector in that space. Quantum mechanically, they are the set of basic (often atomically inspired) functions which are used, in linear combination, to construct the total electronic wavefunctions and/or electron density for a given nuclear framework.<sup>[105]</sup>

When performing DFT calculations, whether it is a single point energy determination or geometry optimisation, the chosen method always consists of a combination of a functional with a basis set, which provides a finite mathematical description of the atomic orbitals. Each basis set is typically comprised of

Gaussian-type basis functions (GTO), with multiple GTOs required to approximate the solution to the Schrödinger equation for the hydrogen atom. Although Slater-type basis sets (STO) provide a more accurate description of the short- and long-range physical behaviour of a hydrogenic orbital, their solution is more computationally demanding, requiring a solution of an infinite series to give the correct answer. Hence, Gaussian-type basis sets are more commonly used to evaluate the electronic structure of organic molecules, with split-valence basis sets providing not only additional efficiency to the speed of calculations, but a better description of valence electron orbitals, which are key for determining the reactivity for a given system.<sup>[106]</sup>

Polar coordinates may be used to express STOs as:

$$\chi_{z,n,l,m}(r,\theta,\varphi) = NY_{l,m} r^{n-1} \exp(-\zeta r) \quad (2.10)$$

where N is a normalization constant,  $Y_{l,m}$  are the spherical harmonics, and  $r^{n-1}$  is the radial part. The exponential dependence on the distance between the nucleus and electron stems from the exact solution of the hydrogen atom. GTO has a similar expression,

$$\chi_{z,n,l,m}(r,\theta,\varphi) = NY_{l,m} r^{2n-2-l} \exp(-\zeta r^2), \dots, \quad (2.11)$$

The Gaussian shape of Eq. 2.4 makes GTOs less accurate than STO. In contrast to STO, which has a discontinuous derivative (cusp), GTO has zero slope at the nucleus, making it difficult for GTOs to accurately reflect behaviour close to the nucleus. Another issue is that, in comparison to STOs, GTOs decay too quickly away from the nucleus, leading to a poor representation of the wavefunction's endpoints. In general, a large number of GTOs must achieve the same STO representation accuracy. Despite these variations, GTOs are more often utilized in computations nowadays than STOs because they provide faster computing of

one- and two-electron integrals. Therefore, the current GTOs are built from a fixed linear-combination of Gaussian functions, contracted GTOs, in order to more accurately depict the cusp in the electron density of the nuclei and have quick calculations at the same time (CGTO).

As already mentioned, the number of functions used affects how accurate basis set is. The smallest possible collection of available functions is referred to as the "minimum foundation set." This uses only the functions that each electron in a neutral atom corresponds to. For instance, hydrogen has just one s-function, but the first-row elements have two s-functions (1s and 2s) as well as p functions (2px, 2py, 2pz). The bare minimal foundation set is sometimes insufficient. A Double Zeta (DZ) basis set is produced by doubling the minimum basis functions, which is an even better improvement. A DZ consists of two s-functions for hydrogen, four s-functions plus two sets of p-functions for the first row of elements, and six s-functions plus four sets of p-functions for the second row of elements. By including more functions, it is possible to produce the Triple Zeta (TZ) and Quadruple Zeta (QZ) basis sets, which each contain three and four times as many functions as the minimum basis. The so-called split valence basis for DZ, TZ, and QZ results from the fact that, in contrast to the norm, only the terms of the valence orbitals increased in this circumstance (VDZ, VTZ, and VQZ). More progress may be achieved by including the key polarizing functions into the explanation of chemical bonding. Adding d-orbitals to p-functions and p orbitals to hydrogen are two examples.<sup>[107]</sup> In contrast to the Triple Zeta plus Double Polarization (TZ2P) type basis, which is created by adding two sets of polarization functions to a TZ basis, the Double Zeta plus Polarization (DZP) type basis is created by adding only one set of polarization functions to the DZ. The Pople family is likely the most well-known of the many basis set families.<sup>[93]</sup> The basis set is designated as k-nlmG, where k is the number of GTOs used for the core orbitals and nml indexes are the quantities used to describe the valence orbitals using functions and GTOs, respectively. As an illustration, in the case of

6-31G, the core orbitals are represented by six GTOs, the inner portion of the valence orbitals by three GTOs, and the outer part of the valence orbitals by one GTO. The inclusion of relativistic effects and the number of core electrons both lengthen the computation process. The Effective Core Potentials (ECP) offer a straightforward remedy (or Pseudopotential). Despite how challenging it is to create, the core idea of ECP is to compute the all-electron wavefunction for an atom using the Dirac-Fock equation.<sup>[108]</sup> Then you need swap out the core potential for a potential parameterized with the proper set of analytical functions (spherical Bessel or Gaussian functions). The parameters of the approximation wavefunction are then changed to match those of the original all-electron wavefunction. For transition metals, the valence orbitals are generally the  $(n + 1)$  s-,  $(n + 1)$  p-, and  $(n)$ d-orbitals, with ECP handling all other orbitals. Although the findings of this approximation are satisfactory, additional (fewer) electrons may be added to or withdrawn from this group. Returning to POMs, it is clear that the employment of ECP would facilitate faster computations due to the abundance of heavy transition metals present in these molecules. Thus We employed the family of ECPs in conjunction with the Hay and Wadt basis set, as explained in the following sections, to represent the inner most and valence electrons of POMs.<sup>[109]</sup>

### 2.6.1 LANL2TZ:

DFT computations frequently use LANL2DZ basis sets. It is common knowledge that the projected ordering of transition metal atomic states clearly demonstrates the inadequacies of the DF approaches in emulating the experimental counter-part. The inaccurate prediction of the energetics of reaction steps and of the binding energy of systems including transition metal is one of the severe effects caused by this constraint. However, it is demonstrated that most of the above-mentioned values may be accurately recreated when certain basis sets are used.

Many of the often-employed effective core potential basis sets are offered by the Stuttgart group and have bigger size basis functions or are of double- or triple-zeta quality. Hay and Wadt created the LANL2TZ basis sets at Los Alamos National Laboratory, which have been extensively employed in quantum chemistry, notably in the investigation of compounds or clusters containing heavy elements<sup>[110]</sup>. The process of fitting pseudo-orbitals using Gaussian functions was used to produce these basis functions.<sup>[111]</sup>

### **2.7 Computational Chemistry:**

Computational chemistry is a subfield of chemistry that makes use of computer simulation to help with chemical problem-solving. For the purpose of calculating the structures and characteristics of molecules, groups of molecules, and solids, theoretical chemistry techniques are incorporated into computer systems. It is crucial since the quantum many-body issue cannot be analytically solved, much less in closed form, with the exception of relatively recent findings on the hydrogen molecular ion (dihydrogen cation). While computational findings often supplement the knowledge gained from chemical experiments, they can occasionally forecast previously unknown chemical processes. It is frequently employed in the development of novel materials and medications. Structure, or the predicted positions of the constituent atoms, absolute and relative (interaction) energies, electronic charge density distributions, dipoles and higher multipole moments, vibrational frequencies, reactivity, or other spectroscopic quantities, and cross sections for collision with other particles are examples of these properties.

Both static and dynamic circumstances are covered by the approaches. In every situation, the size of the system under study leads to a rapid growth in computing time and other resources (such memory and disk space). That system might be solid, collection of molecules, or a single molecule. Very approximate to extremely accurate computational chemistry approaches are available; the latter

is often only practical for tiny systems. Quantum physics and fundamental physical constants serve as the sole foundation for ab initio approaches. Because they employ extra empirical factors, such methodologies are referred to be empirical or semi-empirical.

### 2.8 Computational Methods:

All calculations for geometry optimizations, linear light absorption properties, and first hyperpolarizability NLO ( $\beta$  tensor components) were carried out using the Gaussian16 suite<sup>24</sup> on the High-Performance Computing Cluster supported by the Research and Specialist Computing Support service at the University of East Anglia. Geometry optimizations were carried out utilizing the range-separated hybrid functional  $\omega$ B97XD with the 6-311+G(d) basis set for C, H, N, and O, and on the other hand LANL2TZ basis set for Mo atoms, in accordance with the methodology described in the literature by Rtibi et. al.<sup>[72]</sup> Truhlar and colleagues' SMD solvation model was used to account for solvent effects. The GEN keyword in the Gaussian programming language was used to generate this mixed basis set. In recent years, mixed basis sets of this kind have been increasingly common in computational chemistry research in this field. Both of these basis sets have been frequently employed in conjunction with density functional techniques for investigations of transition metal-containing systems.<sup>[112]</sup> These geometry optimizations were initially performed in the gas phase, and then single point energy using the solvent acetonitrile. TIGHT convergence criteria ( $1.5 \times 10^{-5}$  Hartree/Bohr or Hartree/radian) were applied to the atoms' leftover forces. The same level of theory,  $\omega$ B97XD/6-311+G(d,p)/LANL2TZ, was applied for linear optical calculations using the SMD model for the acetonitrile solvent. Calculations were made for 100 lowest energy transitions with a 50:50 split between singlet and triplet, however only the singlet absorptions turned out to be relevant. Using the same degree of basis set and functional as for optimization and linear optical calculations with acetonitrile



solvent, the NLO characteristics, responses were determined. To further comprehend the charge transfer process and the source of the NLO activity for the investigated compounds, HOMO-LUMO analysis was also carried out. Using the Multiwfn program,<sup>[113]</sup> Guido's charge-transfer lengths ( $r$ ) were calculated in accordance with the method outlined by Guido et. al.<sup>[114]</sup>

### 2.8.1 Hyperpolarizability and Two-State Model Analysis:

To calculate dipole polarizability ( $\alpha$ ) and first-order hyperpolarization ( $\beta$ ), the following equation was applied:

$$\alpha = \frac{1}{3} (\alpha_{xx} + \alpha_{yy} + \alpha_{zz}) \quad (2.12)$$

Whereas for the calculation of static hyperpolarizability ( $\beta_0$ ), the following equations were used:

$$\beta_x = \beta_{xxx} + \beta_{xyy} + \beta_{xzz} \quad (2.13)$$

$$\beta_y = \beta_{yyy} + \beta_{yzz} + \beta_{yxx} \quad (2.14)$$

$$\beta_z = \beta_{zzz} + \beta_{zxx} + \beta_{zyy} \quad (2.15)$$

$$\beta_0 = \sqrt{\beta_x^2 + \beta_y^2 + \beta_z^2} \quad (2.16)$$

Moreover, the SHG responses, specifically the HRS first hyperpolarizability (scattered intensities)  $\beta_{HRS}(-2\omega; \omega, \omega)$  and the static  $\beta_0$  were calculated when the incident light is vertically ( $\langle \beta_{zzz}^2 \rangle$ ) and horizontally ( $\langle \beta_{zxx}^2 \rangle$ ) polarized, respectively, using the following equation:

$$\beta_{HRS}(-2\omega; \omega, \omega) = \sqrt{\langle \beta_{zzz}^2 \rangle + \langle \beta_{zxx}^2 \rangle} \quad (2.17)$$

$\beta$ -responses,  $\beta$ -tensor components of both static  $\beta_0$  and frequency-dependent  $\beta_{HRS}$  (at 1064 nm incident wavelength) were calculated using TD-DFT for optimized

geometries with ωB97XD with the 6-311 + G(d)/LANL2TZ basis sets and SMD scheme to account for solvent effects. For the push-pull  $\pi$ -conjugated system, only a single diagonal tensor component ( $\beta_{zzz}$ ) typically contributes to the  $\beta$  tensor, and hence  $\beta_{HRS}$  can be computed as the following<sup>[72][115]</sup>:

$$\beta_{zzz} = \sqrt{\frac{35}{6}} \beta_{HRS} \quad (2.18)$$

Thus, in this study,  $\beta_{zzz}$  as well as  $\beta_0$  responses have been reported. A two-state approximation is often valid and can be applied for the POM-based derivatives, where  $\beta_{zzz} = \beta$ , which is given by:

$$\beta = \frac{6\Delta\mu_{ge}(\mu_{ge})^2}{(E_{max})^2} \quad (2.19)$$

where Difference in dipole moment between ground (g) state and excited (e) state is  $\mu_{ge} = \mu_e - \mu_g$ , and  $\mu_{ge}$  is the transition dipole moment.  $E_{max} = E_e - E_g$  is the difference in excitation energy between ground (g) state and excited (e) state. Charge-transfer length, Guido's  $\Delta r$ , which measures the electron–hole distance via an analysis of the charge centroids of the orbitals involved in the excitation, are computed following the procedure described by Guido et. al.<sup>[114]</sup> using the Multiwfn software<sup>[113]</sup>.

# **Chapter Three**

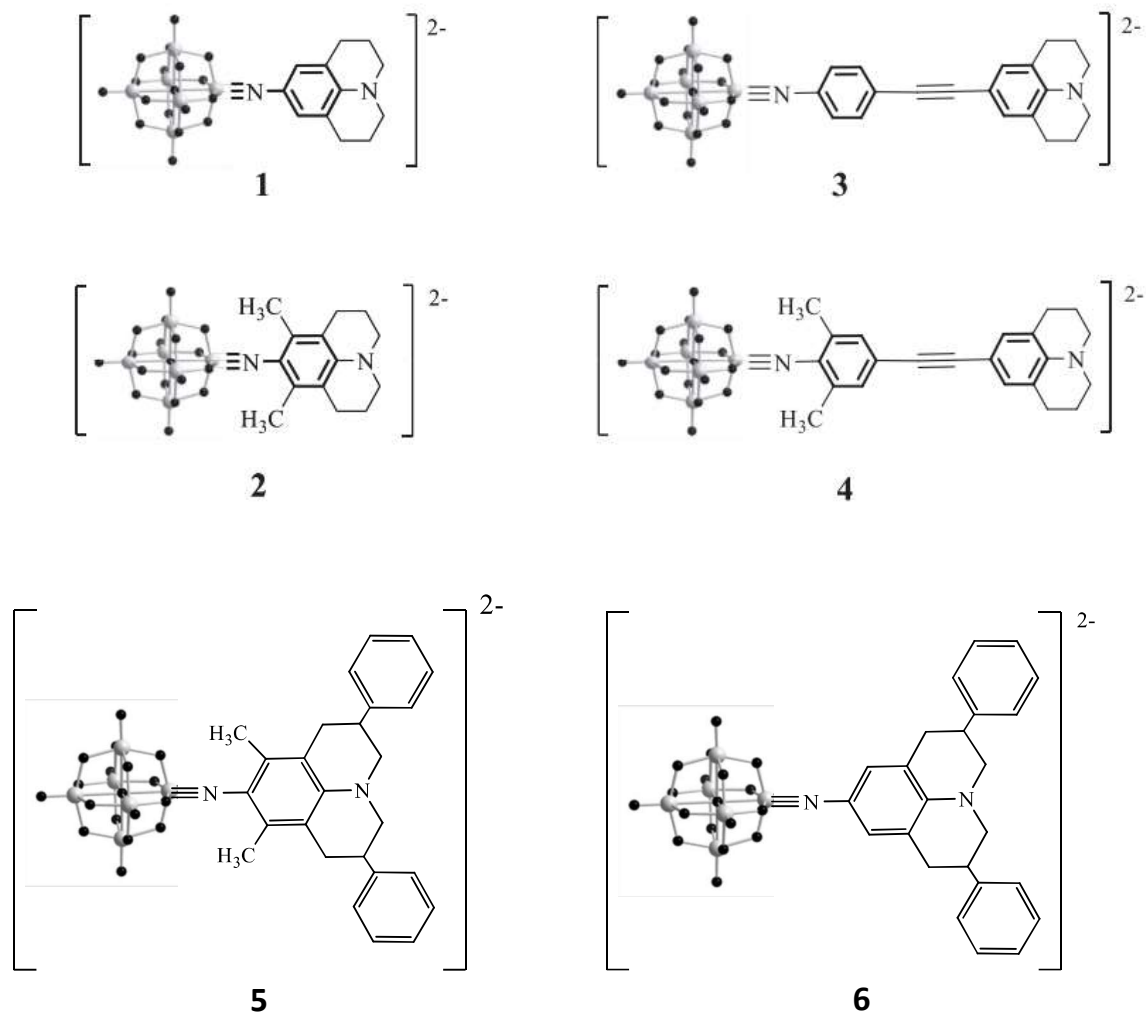
## **Results and Discussions**

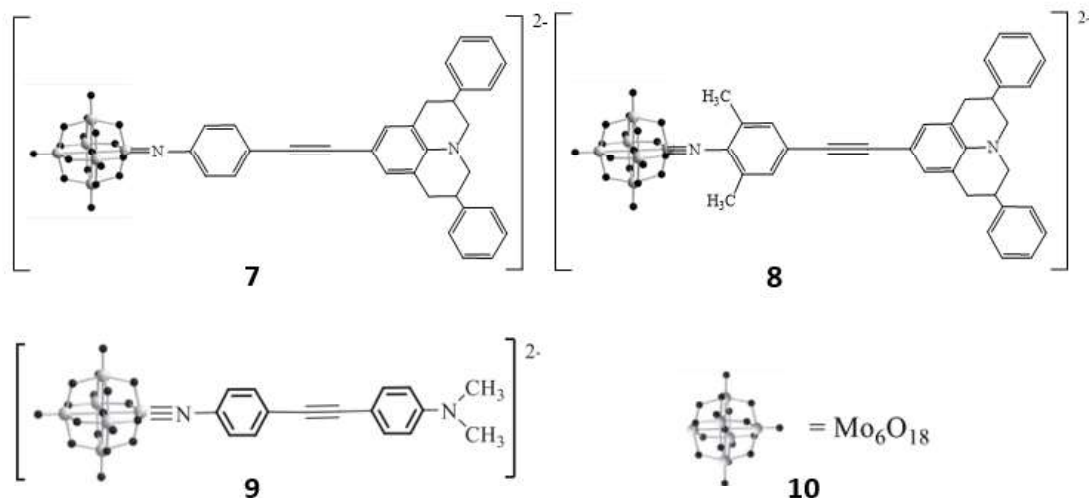
## Chapter Three

## Results and Discussions

## 3. Results and Discussions:

The aim of this project is the development of new organoimido hexamolybdate based on julolidine donor as NLO compounds. This chapter describes the design, and investigation of new series of organoimido Lindqvist derivatives with julolidine donor (scheme 3.1). As far as we know, this is the first study on arylimido-POMs-julolidine derivatives where DFT/TD-DFT studies were used to investigate their electronic structure and linear/nonlinear optical properties.





**Scheme 3.1** Hexamolybdate-organoimido-Julolidine derivatives **1** to **8** investigated in this study.

### 3.1 Ground-State Molecular Geometries For 1 to 4 Compounds:

When the examined compounds **1–4** were optimized at the SMD/ $\omega$ B97XD//6-311 + G(d)/LANL2TZ level of theory, table 3.1 shows some geometrical parameters for their ground-state geometries. The resulting geometries are in accordance with known imido-species, which include imido (Mo $\equiv$ N) bonds that are 1.74–1.76 Å long and an imido angle between 154° and 174° on the Mo=N-C axis. Derivatives **1** and **3** show a lower, more curved, shape.

**Table 3.1** Selected structural parameters where distances are in (Å) and angles in (°) of the geometries of compounds **1** to **4**

Compound	Mo=N-C	Mo=N	N-C	Mo-O <sup>a</sup>	Mo-O <sup>b</sup>
<b>1</b>	154.8	1.75	1.37	2.19	1.69
<b>2</b>	173.7	1.74	1.37	2.21	1.69
<b>3</b>	155.6	1.76	1.36	2.19	1.69
<b>4</b>	170.8	1.75	1.36	2.22	1.69

<sup>a</sup> Central oxygen. <sup>b</sup> Average of Mo–O lengths in calculated structures.

The ortho methyl-substitution to the imido bond may have steric effects that account for the more linear angles of **2** and **4**. In compounds **3** and **4**, the Mo≡N bond is significantly lengthened in comparison to their counterparts **1** and **2** due to increased  $\pi$ -bridge conjugation, but the N–C bond length in these long anions (**3** and **4**) is slightly shortened in comparison to the short derivatives (**1** and **2**). These results support our earlier research.<sup>[15][70][71]</sup> and with Rtibi et al.<sup>[116][72]</sup>. Where methylation is present, as seen in comparisons of **1** with **2**, and **3** with **4**, the Mo≡N bond is slightly compressed by 0.01Å, demonstrating the stabilizing impact of ortho-methylation. The findings of the study of the optimized geometries' free energies, which show that the inclusion of methylation results in a  $\Delta G = -78.54$  Hartree for the case of **1** compared with **2** (methylated analogue) and  $\Delta G = -228.79$  Hartree for **3** and **4**, confirm this. This is in line with our earlier research in which we used an experimental approach to examine the stability of  $C_{2v}$  dumbbell Lindqvist derivatives and found that methylation significantly affects the stability of the imido bond.<sup>[71]</sup>

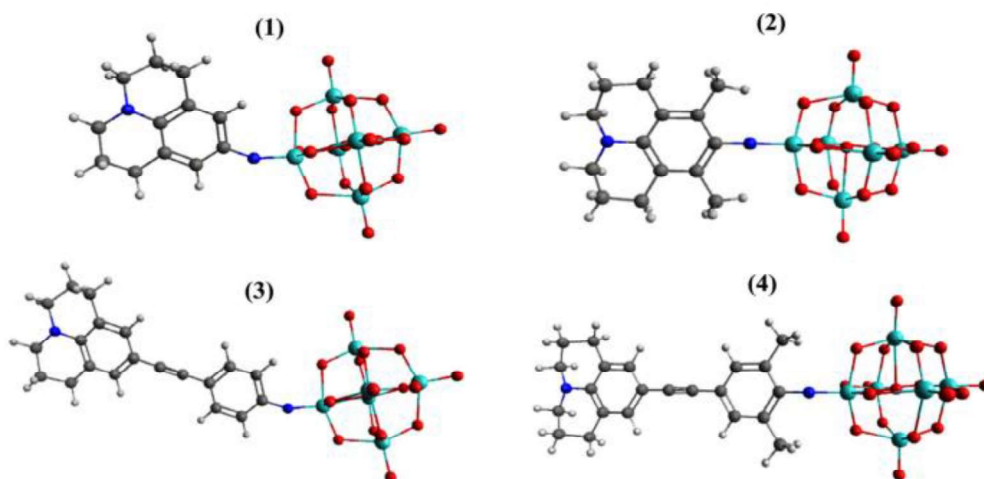


Figure 3.1 Optimized geometries in the solvent phase for anions 1-4. Gray = C, cyan = Mo, white = H, blue = N, and red = O.

### 3.2 NLO Properties: First Hyperpolarizabilities For 1 to 4 Compounds:

It is possible to compare compounds (1-8) static and dynamic initial hyperpolarizabilities at  $\lambda = 1064$  nm in table 3.2, which enables easy comparison with published (experimental) answers. Three of the investigated compounds, **1**, **3**, and **4**, have both the  $\beta_{zzz}$  and  $\beta_0$  values that are significantly higher than those of compound **9** (the reference compound) (both experimentally and theoretically), indicating stronger electronic communication between the POM and julolidine donor group and consequently strong NLO activity. This is explained by the strength of the julolidine group's donor nature when compared to other organic donors in our earlier works.<sup>[15]</sup> The anion with the greatest  $\beta_{zzz}$  and  $\beta_0$  values is **3**, among these anions. The reactions are improved by a factor of 2.1 ( $\approx 1.4$  for 0) when the  $\pi$ -conjugated linker is expanded, as shown when comparing **1** with **3**, and **2** with **4**. In our prior published work, a same trend was seen.<sup>[70]</sup> On the other hand, it was discovered that  $\beta_{zzz}$  and  $\beta_0$  decreased following methylation in anions **2** and **4**, as opposed to **1** and **3**, respectively. The donating impact of the methyl groups, which reduce the energy of the aryl-based orbitals and somewhat enhance the energies of the POM-based orbitals, may be responsible for this, as shown by the study of the HOMO-LUMO energies.

**Table 3.2** Calculated first hyperpolarizabilities (au) of anions **1** to **4** in comparison with experimental and calculated data for compound **9**.

		Calculated <sup>a</sup>		Experimental
		$\beta_0$	$\beta_{zzz}$	$\beta_{zzz}$
		(10 <sup>-30</sup> esu)		
	$\lambda_{\max}$ (nm)	$\lambda=0$	$\lambda=1064$	$\lambda=1064$
<b>1</b>	418	314	483	-
<b>2</b>	402	274	366	-
<b>3</b>	413	464	1048	-
<b>4</b>	408	386	795	-
<b>9</b>	421 <sup>b</sup>	139 <sup>b</sup>	442 <sup>a</sup>	440±55 <sup>b</sup>

Note: The TD-DFT/ $\omega$ B97X-D method was used at the 6-311G\*/LanL2TZ level of theory. <sup>a</sup> Calculated data for **9** from Reference<sup>[116]</sup>. <sup>b</sup> Experimental data for **9** from Reference<sup>[15]</sup>.

### 3.3 UV– Vis Absorption Spectra For 1 to 4 Compounds:

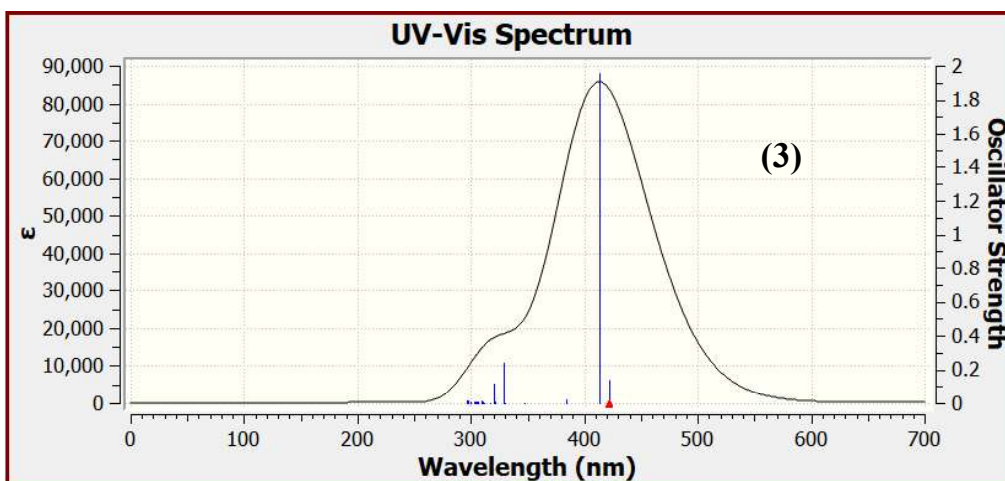
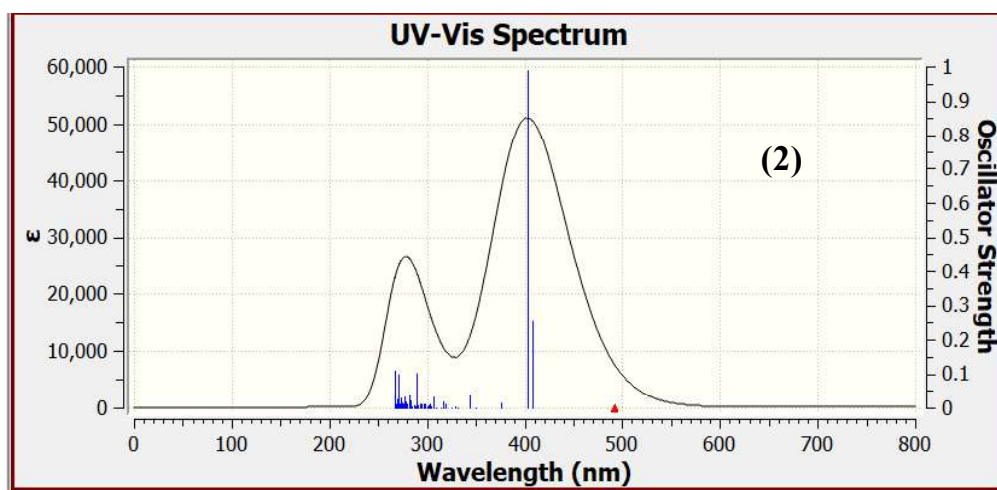
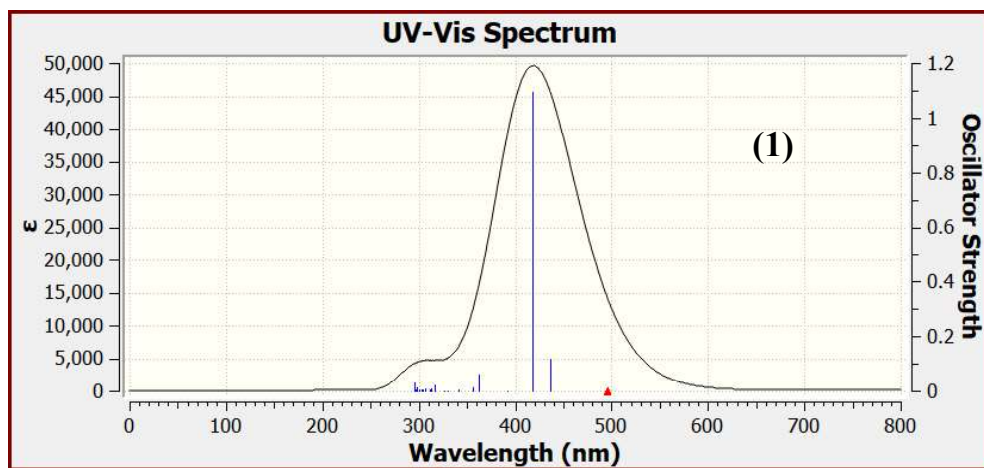
Calculations of UV-vis absorption qualities were done in order to comprehend the orbital transition properties linked to important excited states of dipolars. Using TD-DFT computations in an acetonitrile solvent, the lowest 100 transitions were calculated using a 50:50 mixture of singlet and triplet transition states (table 3.3). Table 3.3 displays the oscillator strengths, transition types, and maximum absorption wavelengths ( $\lambda_{\max}$ ) values ( $f_{os}$ ). Just one excited state, with oscillator strength of at least one, contributes to the low energy absorption band for each of the species under investigation. All transition energies slightly increased after methylation, showing a minor drop in the energies of the aryl-based orbitals and a slight rise in the energies of the POM-based orbitals, when comparing **1** and **3** with their ortho-methylated equivalents **2** and **4**, respectively. This is in line with the methylated counterparts' wider HOMO-LUMO gap. The examined systems (**1-4**) all display a minor blue shift in  $\lambda_{\max}$  with respect to reference compound **5**, along with improved NLO responses, indicating superior transparency/non-linearity trade-offs for these systems.

The HOMO/HOMO-1 involved in the transitions for lengthy anions (**3** and **4**) covers the full arylimido unit with some POM character. The HOMO is likewise distributed over the arylimido unit with some POM character in the short dipolars (**1** and **2**), in contrast to HOMO-1, which is fully arylimido-based. In every species, the LUMO acceptor orbital is solely reliant on POM. The POM orbitals, certain imido group orbitals, and the  $\pi^*$  aryl-bridge orbitals all play a key role in the distinctive characteristics of the LUMO+x acceptor orbitals. This demonstrates unequivocally that the POM participates in electronic transitions as an acceptor, producing substantial charge transfer characteristics. Also, the



appearance of hybrid delocalized orbitals that extend from the julolidine to the POM group (extension of CT) suggests that compound **4** introduction of the strong donor, julolidine, is what caused the increase in second order NLO activity. However, for short dipolars, a change in the main contributor to the strongest transition, which is HOMO→LUMO+8 in **1** and HOMO→LUMO+17 in **2**, was seen upon methylation (2.96 eV in **1**, 3.08 eV in **2**, but both having almost the same  $f_{os}$ ), indicating an increase in the amount of POM character in the transitions of **2** along with a higher degree of charge separation. This may be explained by the donation effect of the methyl groups, which reduces the energy of aryl-based orbitals more than POM-based orbitals, supporting the observed shorter and less curved, more linear imido-bond in **2** and **4**.

For the reference compound (**9**),  $\Delta\mu_{ge}$  is 15.23 D with a  $d_{CT}$  (charge-transfer distance) of 4.78 Å, and a  $\mu_{ge}$  of 5.20 eV. Moving to compound **3**, which has the largest response of the test species,  $\Delta\mu_{ge}$  is higher than **9**, **2**, and **4**, with a greater charge transfer length ( $\Delta r = 10.38$  Å). Additionally, the  $\mu_{ge}$  is about 2.5 times larger than that of **9**, at 13.10 eV, with a smaller HOMO–LUMO gap (5.3 eV). The corresponding  $\Delta r$  of **3** bridges over the julolidine moiety and the entirety of the POM cluster, indicating strong electronic transition from the donor to the POM (Figure3.6). These variations, in addition to the reduction in the first excitation energy, are characteristic of improved push-pull  $\pi$ -conjugated character, and which hence lead to an increase in the  $\beta$  values. For compounds **1**, **2**, and **4**,  $\Delta r$  and  $\Delta\mu_{ge}$  (except for **4**) are lower than **3** with larger HOMO-LUMO gaps, and whilst  $\Delta r$  also involves julolidine this only goes up to the first atoms of the POM, and so are less delocalized compared to compound **3**, which is consistent with their relative decreases in  $\beta$  responses.



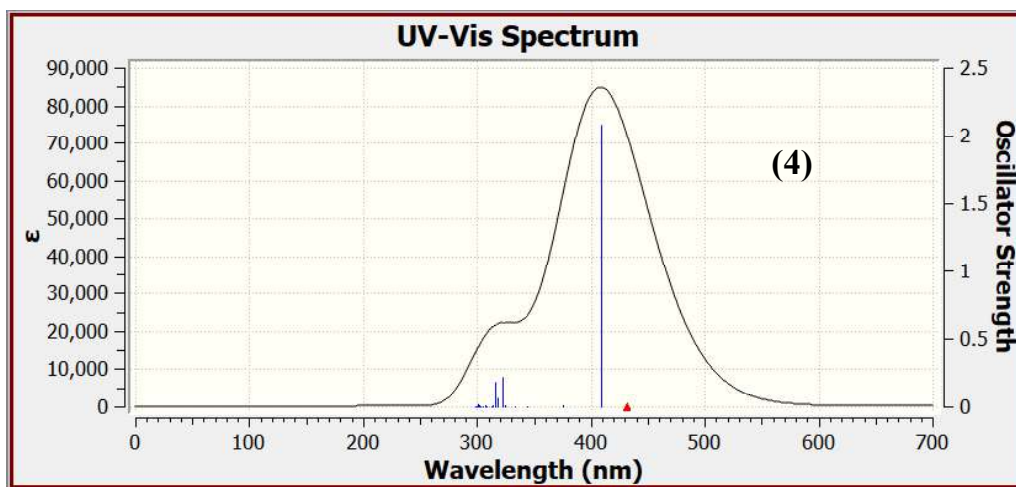


Figure 3.2 UV-Vis spectra calculated by TD-DFT for 1,2,3,4 respectively.

Table 3.3 Calculated maximum absorption wavelength ( $\lambda_{\max}$ ), electronic transition energy ( $E_{\max}$ ), oscillator strength ( $f_{os}$ ), and the percentage MO contribution.

Comp.	n	$\lambda_{\max}$ , nm	$E_{\max}$ eV	$f_{os}$	$\Delta\mu_{ge}$ , D	$E_{\text{HOMO-LUMO}}$ gap, eV	$\mu_{ge}$ , D	$\Delta r$ , Å	Transition	Con. %
1	2	436	2.84	0.11	16.5169	5.46	3.31	6.47	HOMO-2→LUMO+5	3
									HOMO-2→LUMO+13	6
									HOMO→LUMO	3
									HOMO→LUMO+2	12
									HOMO→LUMO+5	18
									HOMO→LUMO+8	4
									HOMO→LUMO+13	24
	3	418	2.96	1.09	16.5169	5.46	9.85	6.42	HOMO→LUMO+2	12
									HOMO→LUMO+4	15
									HOMO→LUMO+5	4
									HOMO→LUMO+6	13
									HOMO→LUMO+8	20
									HOMO→LUMO+10	5
									HOMO→LUMO+13	4
2	2	407	3.03	0.25	15.48	5.58	4.69	6.71	HOMO-2→LUMO+13	5
									HOMO→LUMO	3
									HOMO→LUMO+2	6
									HOMO→LUMO+3	7
									HOMO→LUMO+4	7
									HOMO→LUMO+6	16
									HOMO→LUMO+8	5
									HOMO→LUMO+17	21

									HOMO→LUMO+6	6		
									HOMO-2→LUMO+5	3		
	3	402	3.08	0.98			9.18	6.45	HOMO→LUMO+5	37		
									HOMO→LUMO+7	4		
									HOMO→LUMO+8	20		
									HOMO→LUMO+13	7		
3	1	421	2.93	0.13	16.42	5.3	3.51	8.27	HOMO-1→LUMO	13		
									HOMO-1→LUMO+3	13		
									HOMO-1→LUMO+4	14		
									HOMO-1→LUMO+7	7		
									HOMO→LUMO	9		
	2	413	2.99	1.95			13.1	10.4	13.1	10.4	HOMO→LUMO+3	6
											HOMO→LUMO+4	9
											HOMO-1→LUMO+2	22
											HOMO-1→LUMO+8	5
											HOMO→LUMO+2	32
4	2	408	3.03	2.08	15.54	5.48	13.4	9.8	HOMO→LUMO+4	3		
									HOMO-1→LUMO+6	3		
									HOMO→LUMO+8	10		
									HOMO-1→LUMO+1	2		
	7	322	3.83	0.21			3.86	8.04	3.86	8.04	HOMO-1→LUMO+2	15
											HOMO-1→LUMO+4	8
											HOMO-1→LUMO+8	5
											HOMO-1→LUMO+1	3
								HOMO→LUMO+2	23			
								HOMO→LUMO+4	14			
								HOMO→LUMO+8	10			
								HOMO-5→LUMO	5			
								HOMO→LUMO	9			
								HOMO→LUMO+4	8			
								HOMO-1→LUMO	9			
								HOMO-1→LUMO+2	9			
<b>9, ref</b>	2	421	3.25	2.15	15.23	-	5.2	4.78 <sup>a</sup>	-	-		

<sup>a</sup> The value is charge-transfer distance (dCT) which measures the distance between the barycenters of density gain and depletion upon excitation.<sup>[117]</sup>

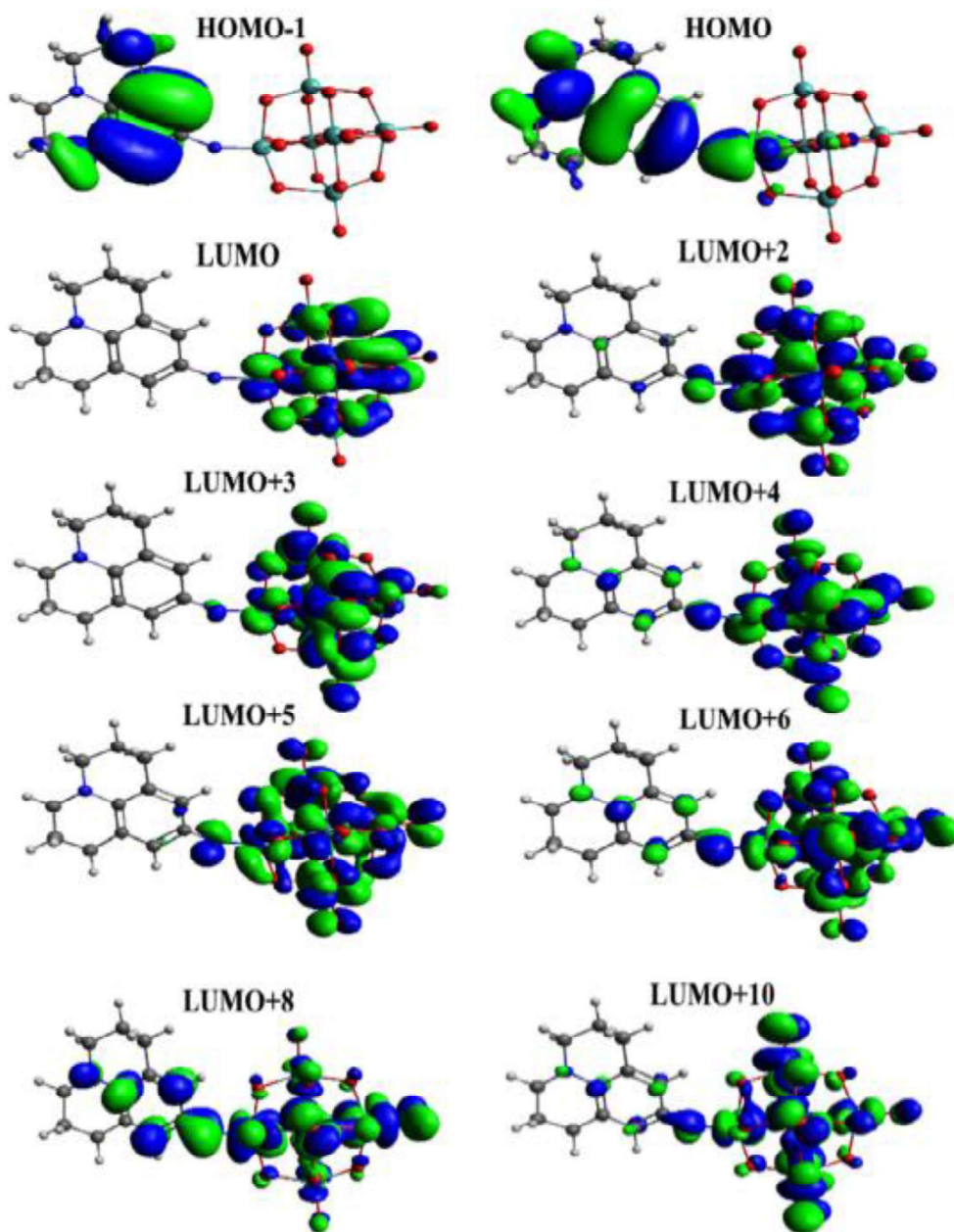


Figure 3.3 The molecular orbitals involved in significant transitions of 1.



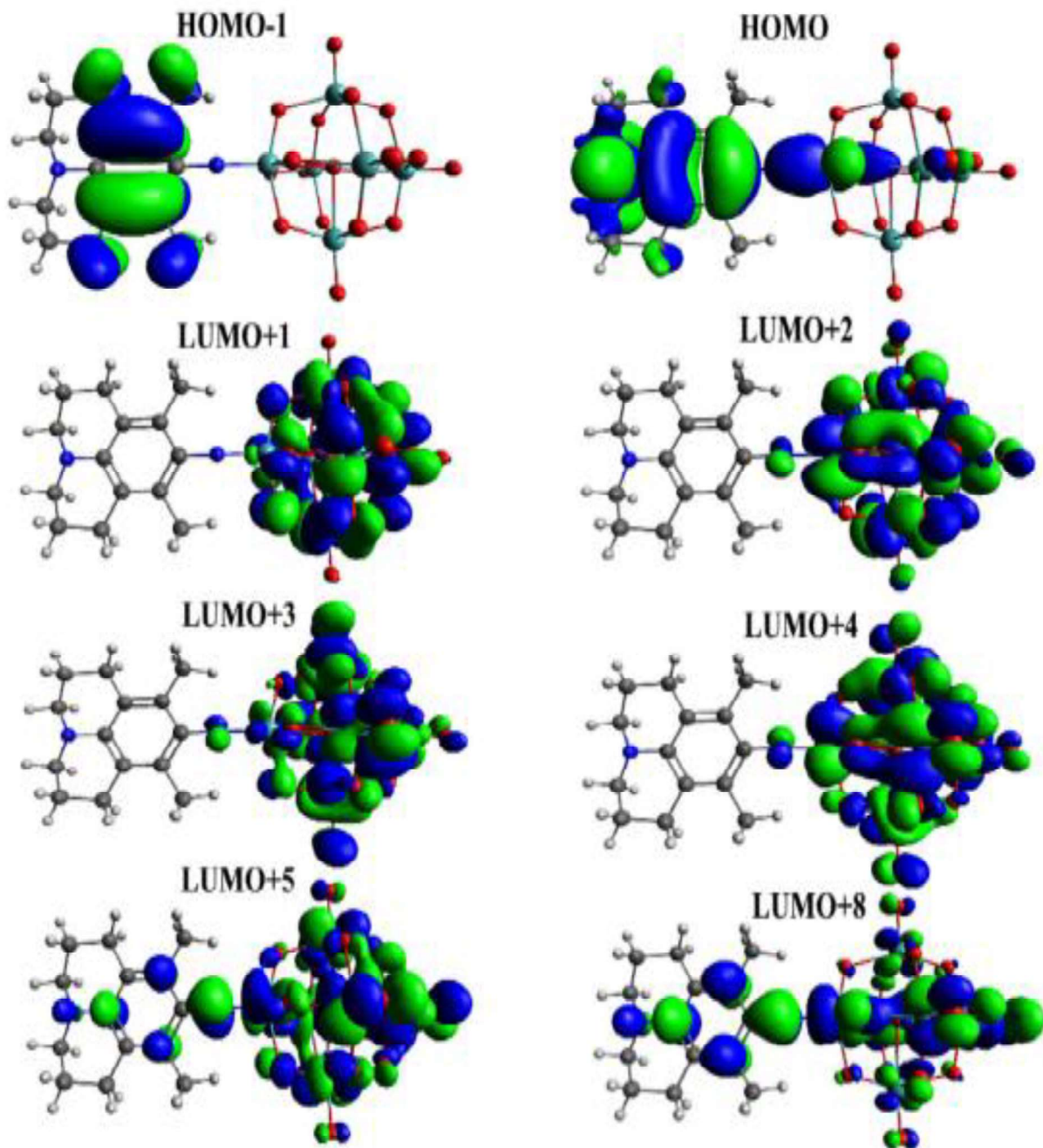


Figure 3.4 The molecular orbitals involved in significant transitions of 2.

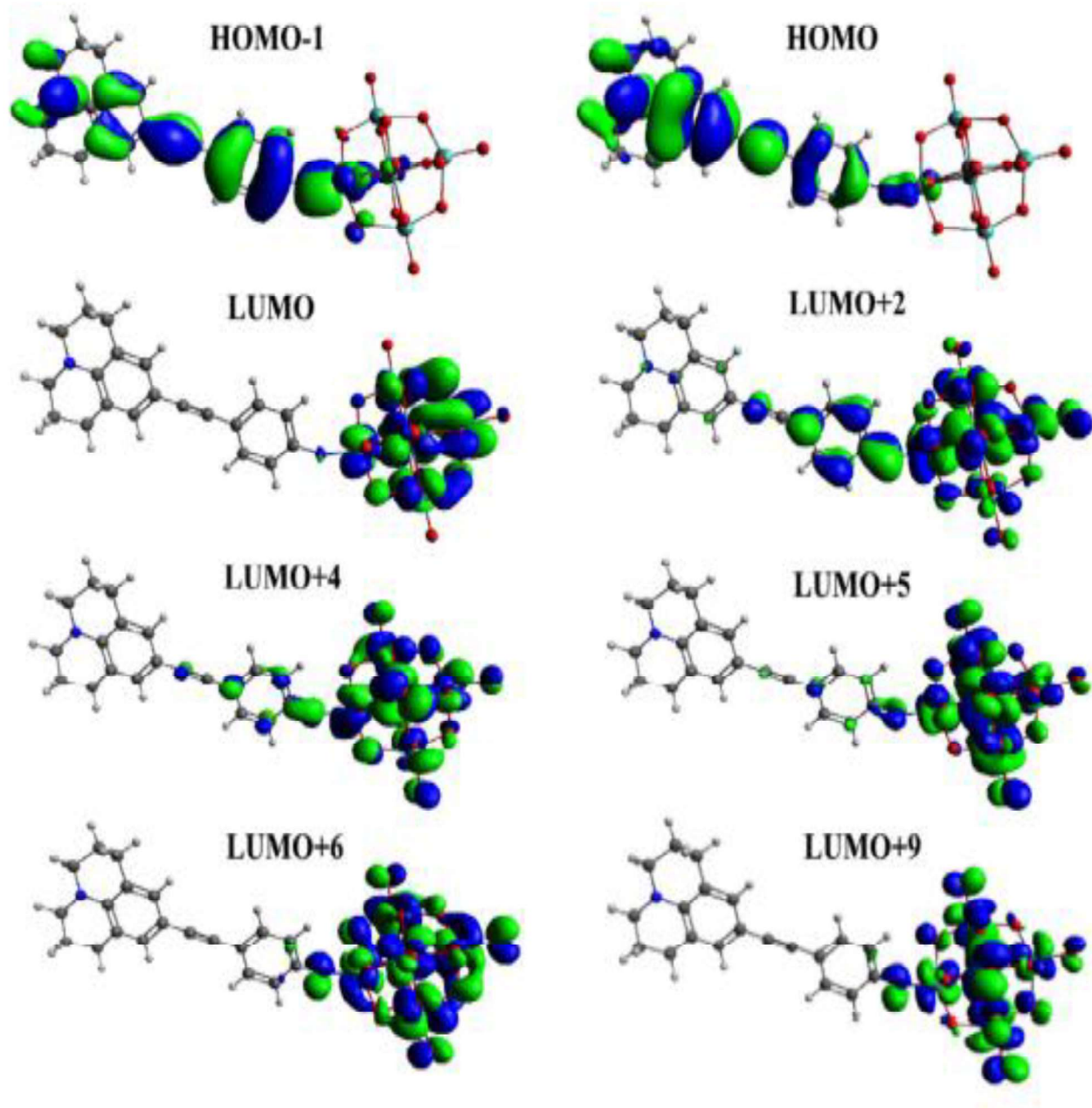


Figure 3.5 The molecular orbitals involved in significant transitions of 3.

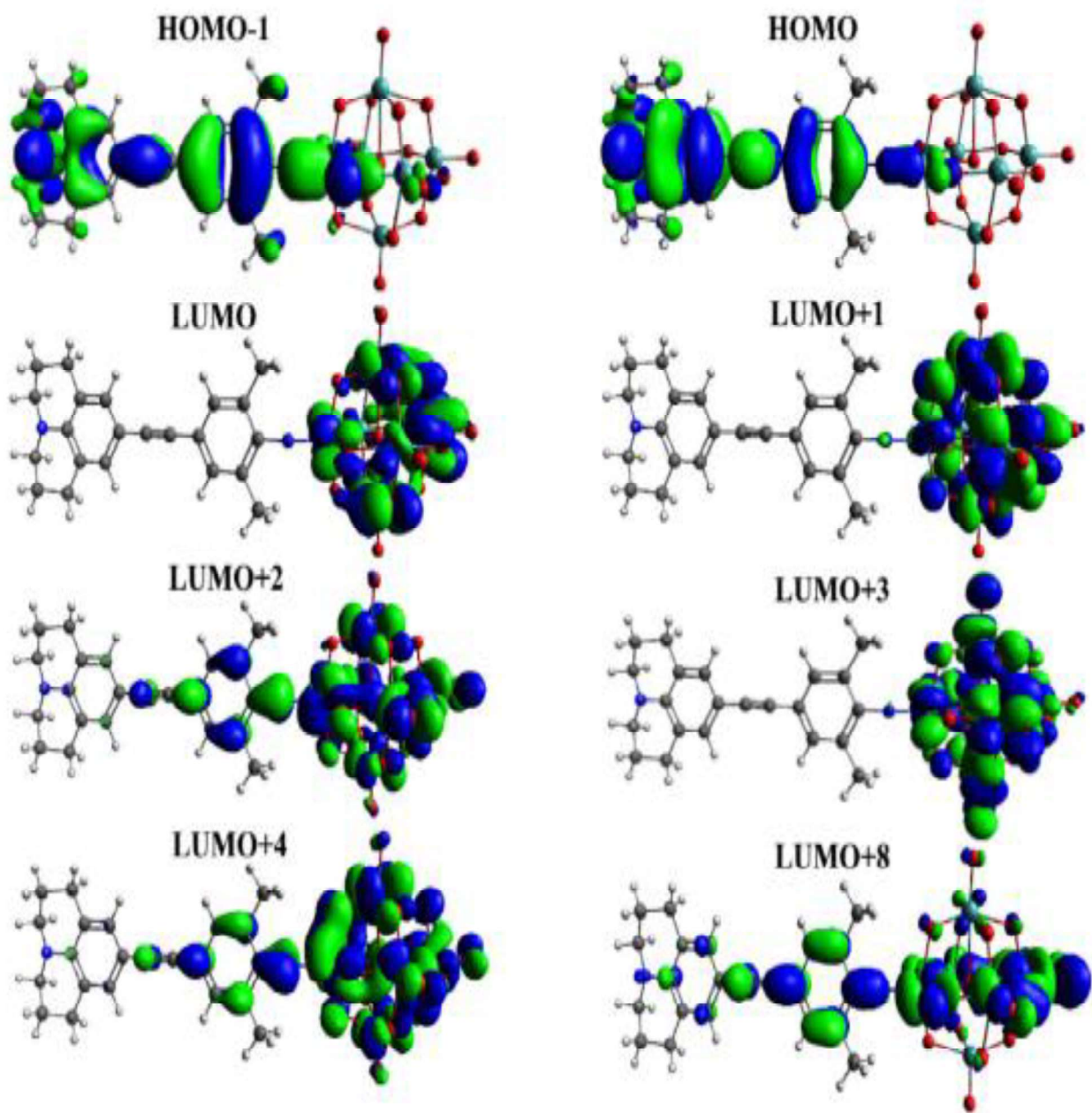


Figure 3.6 The molecular orbitals involved in significant transitions of 4.



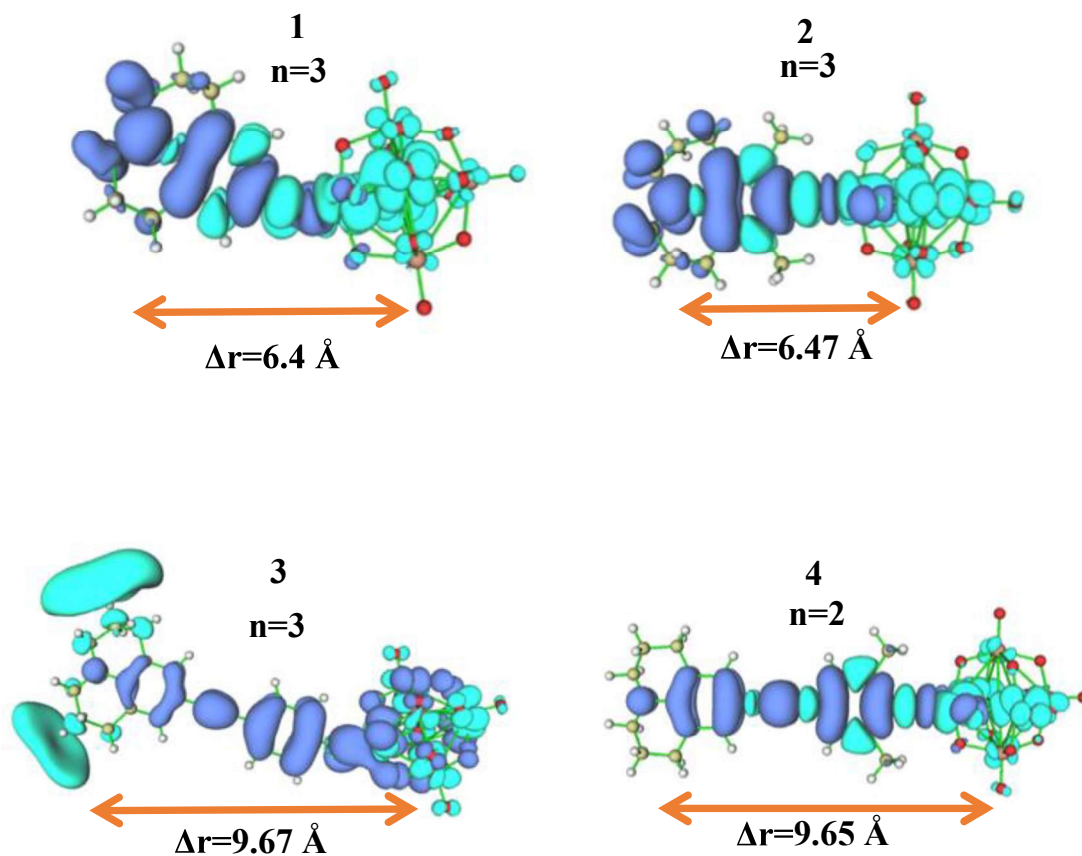


Figure 3.7 Excitation-induced charge density difference ( $\Delta r$ ) for key excited states of compounds 1-4 (isovalue = 0.0003 au; light/dark blue corresponds to positive/negative  $\Delta r$  so that the excitation-induced electron transfer goes from dark to light blue).

### 3.4 Effects of Substituents of Julolidine:

In order to deduce structure-property relationships and to farther tune the NLO responses of derivatives under study, modulation of the Julolidine-donor character by changing the substituent on the 2, and 6 position of the julolidine with phenyl groups (compounds **5-8** in scheme 3.1) was also investigated.

#### 3.4.1 Ground-State Molecular Geometries For **5** to **8** Compounds:

The examined compounds **5-8** were optimized at the SMD/ $\omega$ B97XD//6-311 + G(d)/LANL2TZ level of theory. Table 3.4 shows some geometrical parameters for their ground-state geometries. The resulting geometries are in accordance with known imido-species, which include imido (Mo $\equiv$ N) bonds that are 1.74–1.76 Å long and an imido angle between 153° and 174° on the Mo=N-C axis. Derivatives **5** and **7** show a lower, more curved, shape which could be attributed to the donor strength.

**Table 3.4** Selected structural parameters where distances are in (Å) and angles in (°) of the geometries of compounds **5-8**.

Compound	Mo=N-C	Mo $\equiv$ N	N-C	Mo-O <sup>a,c</sup>	Mo-O <sup>b</sup>
<b>5</b>	153.9	1.75	1.37	2.18	1.69
<b>6</b>	174	1.74	1.37	2.21	1.69
<b>7</b>	155.3	1.76	1.36	2.19	1.69
<b>8</b>	170.6	1.75	1.36	2.21	1.69

<sup>a</sup> Central oxygen. <sup>b</sup> Average of Mo–O lengths in calculated structures.

The ortho methyl-substitution to the imido bond may have steric effects that account for the more linear angles of **6** and **8**. In compounds **7** and **8**, the Mo $\equiv$ N bond is significantly lengthened in comparison to their counterparts **5** and **6** due to the increased  $\pi$ -bridge conjugation, but the N–C bond length in these long anions (**7** and **8**) is slightly shortened in comparison to the short derivatives (**5** and **6**). Where methylation is present, as seen in comparisons of **5** with **6**, and **7** with **8** the Mo $\equiv$ N bond is slightly compressed by 0.01Å, demonstrating the

stabilizing impact of ortho-methylation. The findings of the study of the optimized geometries' free energies, which show that the inclusion of methylation results in a  $\Delta G = -78.63$  Hartree for the case of **6** compared with **5** (methylated analogue) and  $\Delta G = -78.64$  Hartree for **8** and **7**, confirm this. This is in line with our earlier results for derivatives **1-4**, and is consistent with results by AlYasari *et.al* in which an experimental approach to examine the stability of  $C_{2v}$  dumbbell Lindqvist derivatives and find that methylation significantly affects the stability of the imido bond.

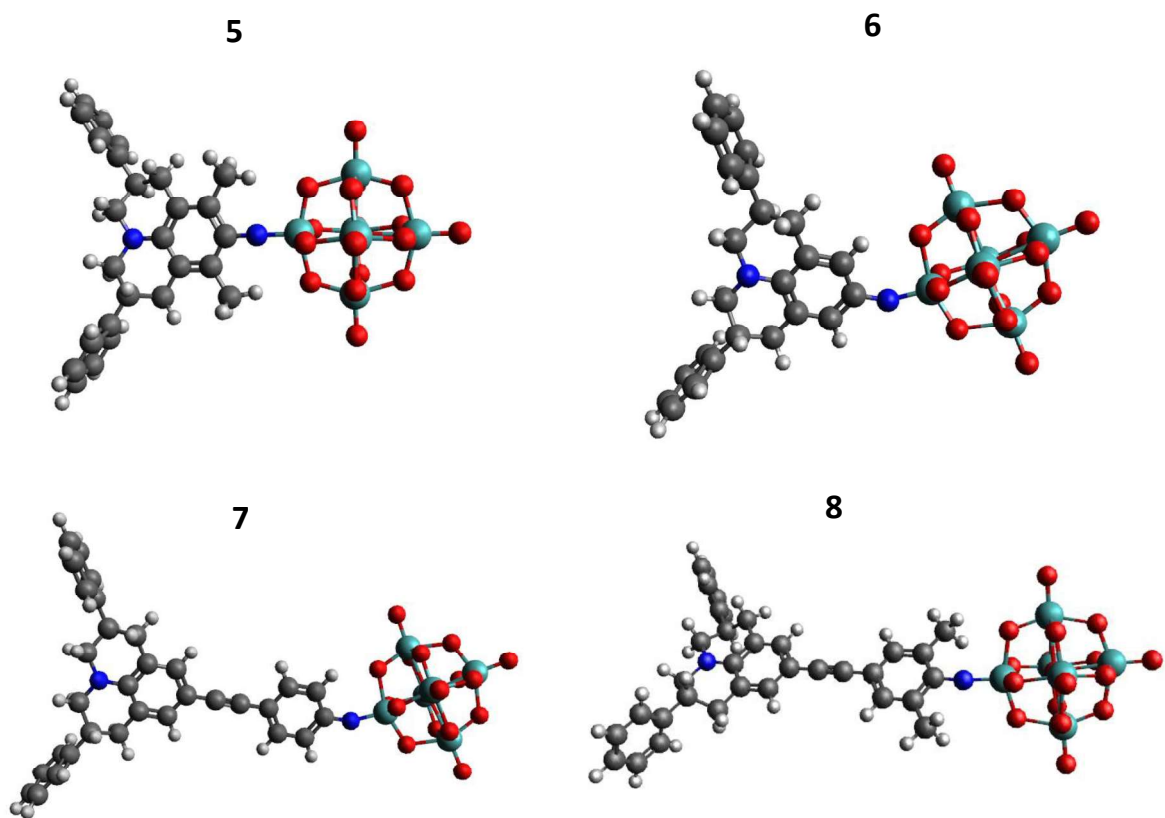


**Figure 3.8** Optimized geometries in the solvent phase for anions **1-4**. Gray = C, cyan = Mo, white = H, blue = N, and red = O.

### 3.4.2 NLO Properties: First Hyperpolarizabilities For 5 to 8 Compounds:

It is possible to compare compounds **5** through **9** static and dynamic initial hyperpolarizabilities at  $\lambda = 1064$  nm, shown in table 3.5, which enables easy comparison with published (experimental) results. Three of the investigated compounds, **6**, **8**, and **9**, have both the  $\beta_{zzz}$  and  $\beta_0$  values that are significantly higher than those of compound **5** (the reference compound) (both experimentally and theoretically), indicating stronger electronic communication between the POM and julolidine donor group and consequently strong NLO activity. This is explained by the strength of the julolidine group's donor nature when compared to other organic donors in our earlier works.<sup>[15]</sup> Among these anions, the greatest  $\beta_{zzz}$  and  $\beta_0$  values is for **8**. The response is improved by a factor of 2.1 ( $\approx 1.4$  for  $\beta_0$ ) with minimal change in  $\lambda_{\max}$  when the  $\pi$ -conjugated linker is expanded, as shown when comparing **5** with **7**, and **6** with **8**. In our prior published work, a same trend was seen.<sup>[70]</sup> On the other hand, it was discovered that  $\beta_{zzz}$  and  $\beta_0$  decreased following methylation in anions **6** and **8**, as opposed to **5** and **7**, respectively. The donating impact of the methyl groups, which reduce the energy of the aryl-based orbitals and somewhat enhance the energies of the POM-based orbitals, may be responsible for this, as shown by the study of the HOMO-LUMO energies.

**Table 3.5** Calculated first hyperpolarizabilities (au) of anions 5–8 in comparison with experimental and calculated data for compound 9.

		Calculated <sup>a</sup>		Experimental
		$\beta_0$	$\beta_{zzz}$	$\beta_{zzz}$
		(10 <sup>-30</sup> esu)		
	$\lambda_{\max}$ (nm)	$\lambda=0$	$\lambda=1064$	$\lambda=1064$
<b>5</b>	418	313	548	-
<b>6</b>	412	345	533	-

<b>7</b>	412	456	1172	-
<b>8</b>	418	485	1242	-
<b>9</b>	421 <sup>b</sup>	139 <sup>b</sup>	442 <sup>a</sup>	440±55 <sup>b</sup>

Note: The TD-DFT/ $\omega$ B97X-D method was used at the 6-311G\*/LanL2TZ level of theory. <sup>a</sup> Calculated data for **9** from Reference<sup>[116]</sup>. <sup>b</sup> Experimental data for **9** from Reference<sup>[15]</sup>.

### 3.4.3 UV–Vis Absorption Spectra For **5** to **8** Compounds:

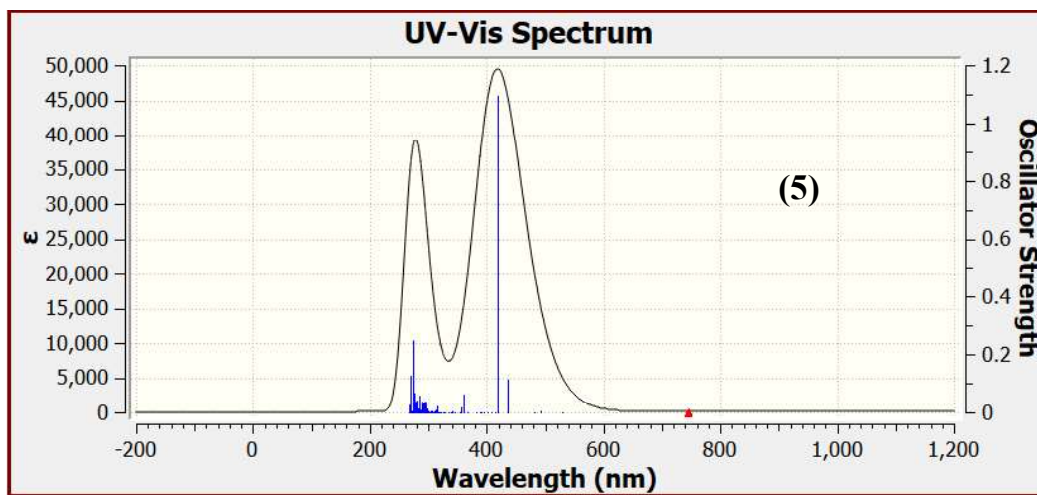
Table 3.5 and figure 3.9 displays the oscillator strengths values ( $f_{os}$ ), transition types, and maximum absorption wavelengths ( $\lambda_{max}$ ). Just one excited state, with oscillator strength of at least one, contributes to the low energy absorption band for each of the species under investigation. All transition energies slightly increased after methylation, showing a minor drop in the energies of the aryl-based orbitals and a slight rise in the energies of the POM-based orbitals, when comparing **5** and **7** with their ortho-methylated equivalents **6** and **8**, respectively. This is in line with the wider HOMO-LUMO gap for methylated derivatives. The examined systems (**5-8**) all display a minor blue shift in  $\lambda_{max}$  with respect to reference compound **9**, along with improved NLO responses, indicating superior transparency/non-linearity trade-offs for these systems over comparable organic pure compounds.

The HOMO/HOMO-1 involved in the transitions for long anions (**7** and **8**) covers the full arylimido unit with some POM character. The HOMO is likewise distributed over the arylimido unit with some POM character in the short dipolars (**5** and **6**), in contrast to HOMO-1, which is fully arylimido-based (figures 2–5). In every species, the LUMO acceptor orbital is solely reliant on POM. The POM orbitals, certain imido group orbitals, and the  $\pi^*$  aryl-bridge orbitals all play a key role in the distinctive characteristics of the LUMO+x acceptor orbitals. This demonstrates unequivocally that the POM participates in electronic transitions as an acceptor, producing substantial charge transfer characteristics. Also, the appearance of hybrid delocalized orbitals that extend from the julolidine to the

POM group (extension of CT) suggests that compound **8** where introduction of the strong donor, julolidine, is what caused the increase in second order NLO activity. However, for short dipolars, a change in the main contributor to the strongest transition, which is HOMO→LUMO+9 in **6** and HOMO→LUMO+8 in **5**, was seen upon methylation, indicating an increase in the amount of POM character in the transitions of **6** along with a higher degree of charge separation. This may be explained by the donation effect of the methyl groups, which reduces the energy of aryl-based orbitals more than POM-based orbitals, supporting the observed shorter and less curved, more linear imido-bond in **6** and **8**.

For the reference compound **9**,  $\Delta\mu_{ge}$  is 15.23 D with a  $d_{CT}$  (charge-transfer distance) of 4.78 Å, and a  $\mu_{ge}$  of 5.20 eV. Moving to compound **8**, which has the largest response of the test species,  $\Delta\mu_{ge}$  is higher than **5-7** and **9**, with a greater charge transfer length ( $\Delta r = 9.65$  Å). Additionally, the  $\mu_{ge}$  is about 2.5 times larger than that of **9**, at 13.97 eV, with a smaller HOMO–LUMO gap (5.34 eV).

The corresponding  $\Delta r$  of **5-8** derivatives bridges over the julolidine moiety and the entirety of the POM cluster, indicating strong electronic transition from the donor to the POM (figure3.12). These variations, in addition to the reduction in the first excitation energy, are characteristic of improved push-pull  $\pi$ -conjugated character leading to an increase in the  $\beta$  values.



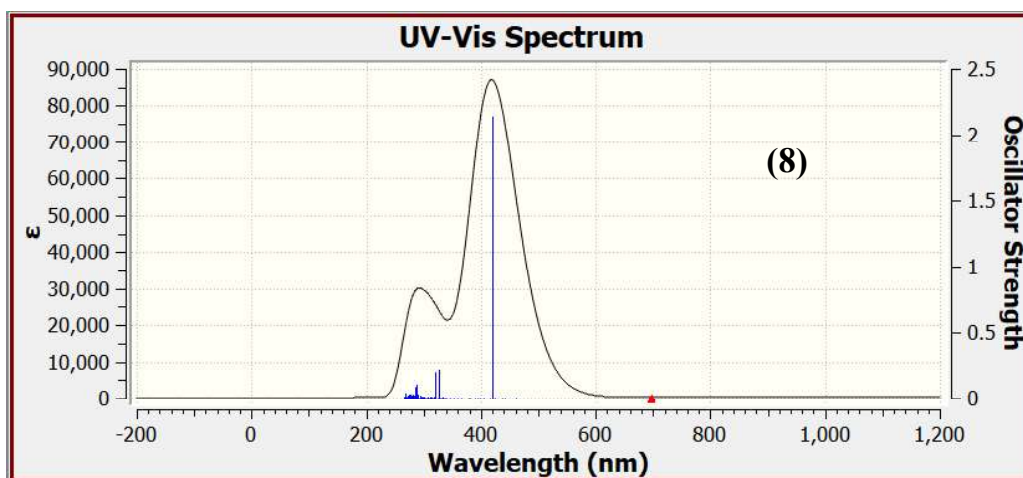
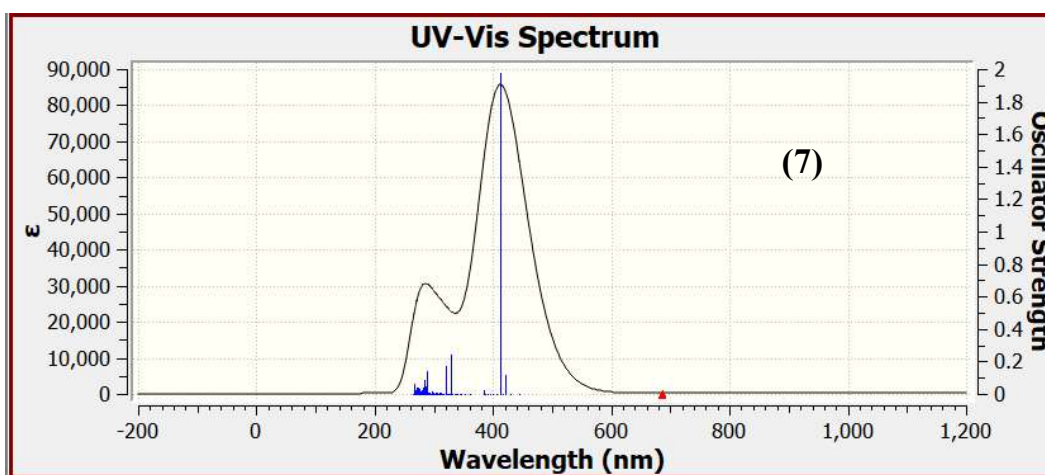
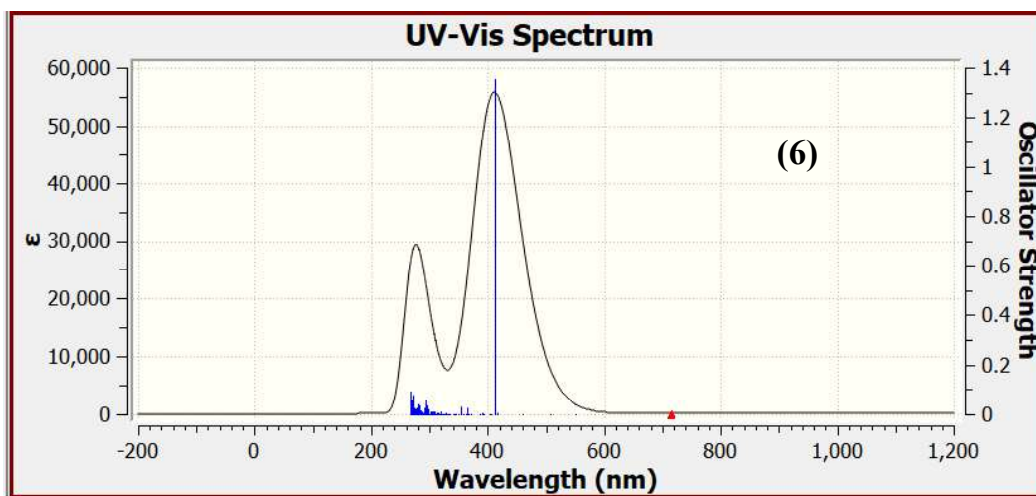


Figure 3.9 UV-Vis spectrum calculated theoretically for 5,6,7,8 respectively.

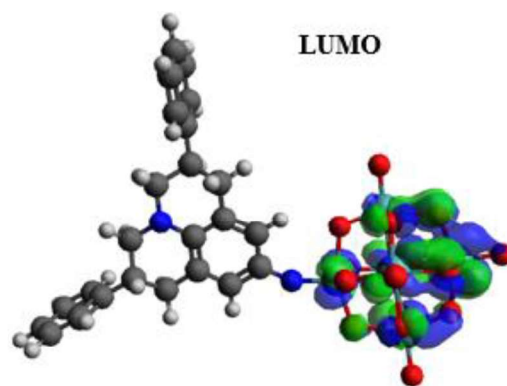
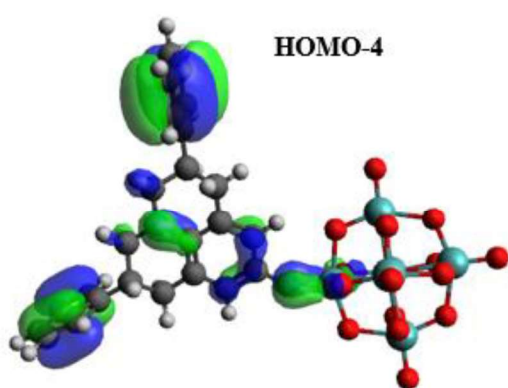
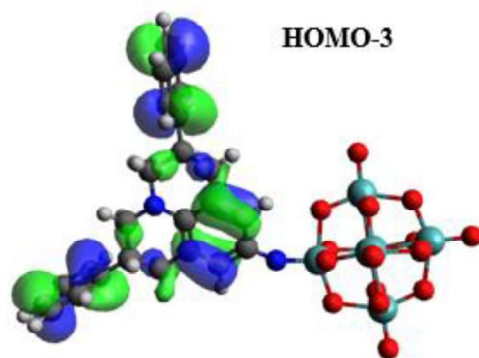
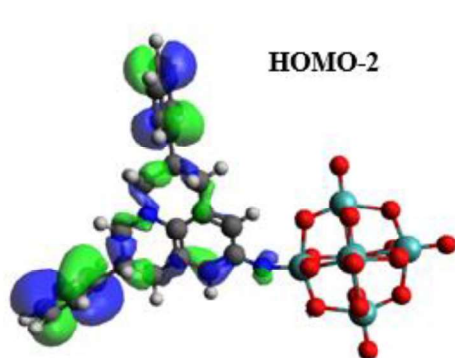
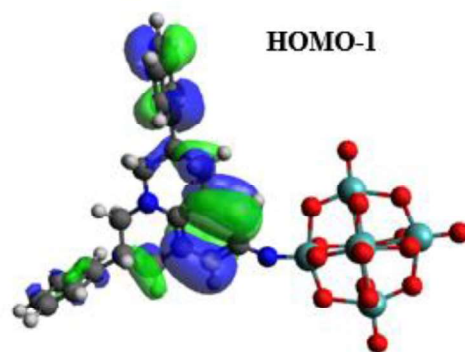
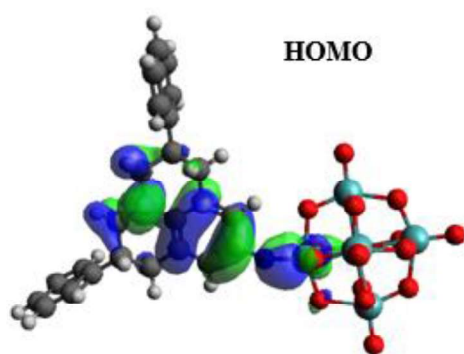
Table 3.6 Calculated maximum absorption wavelength ( $\lambda_{\max}$ ), oscillator strength ( $f_{os}$ ), electronic transition energy ( $E_{\max}$ ), and the percentage MO contribution.

Comp.	n	$\lambda_{\max}$ , nm	$E_{\max}$ eV	$f_{os}$	$\Delta\mu_{ge}$ , D	$E_{\text{HOMO-LUMO}}$ gap, eV	$\mu_{ge}$ , D	$\Delta r$ , Å	Transition	Con. %
5	6	418.04	2.69	1.09	22.26	5.49	9.85	6.4	HOMO→LUMO+2	10
									HOMO→LUMO+3	10
									HOMO→LUMO+4	13
									HOMO→LUMO+5	3
									HOMO→LUMO+6	13
									HOMO→LUMO+7	2
									HOMO→LUMO+8	19
									HOMO→LUMO+10	4
	89	274.71	4.51	0.24	22.26	5.49	3.81	6.4	HOMO→LUMO+13	4
									HOMO-12→LUMO+2	6
									HOMO-12→LUMO+3	3
									HOMO-9→LUMO+2	2
									HOMO-7→LUMO+2	2
									HOMO-7→LUMO+5	10
									HOMO-7→LUMO+7	2
									HOMO-7→LUMO+13	4
HOMO→LUMO+9	4									
HOMO→LUMO+11	4									
6	7	412.62	3	1.35	22.67	5.449	10.88	6.47	HOMO→LUMO+3	17
									HOMO→LUMO+5	24
									HOMO→LUMO+6	5
									HOMO→LUMO+9	27
									HOMO→LUMO+10	2
									HOMO→LUMO+11	2
	99	268.02	4.62	0.09	22.67	5.449	2.31	6.47	HOMO-7→LUMO+7	2
									HOMO→LUMO+9	27
									HOMO→LUMO+10	4
									HOMO→LUMO+11	5
									HOMO→LUMO+12	13
									HOMO→LUMO+13	4
7	7	412.66	3	1.97	22.84	5.338	13.15	9.67	HOMO-1→LUMO+2	22
									HOMO-1→LUMO+5	2
									HOMO-1→LUMO+8	5
									HOMO→LUMO+2	32
									HOMO→LUMO+4	3
									HOMO→LUMO+5	3
	24	328	3.78	0.24	22.84	5.338	4.12	9.67	HOMO→LUMO+8	10
									HOMO-16→LUMO	3
									HOMO-9→LUMO+2	4
									HOMO-8→LUMO	2



									HOMO-1→LUMO	4	
									HOMO-1→LUMO+2	14	
									HOMO-1→LUMO+5	4	
									HOMO-1→LUMO+6	2	
									HOMO→LUMO	3	
									HOMO→LUMO+4	7	
									HOMO→LUMO+5	9	
									HOMO→LUMO+8	4	
									HOMO→LUMO+17	2	
									HOMO→LUMO+19	5	
<b>8</b>	6	418.87	2.96	2.13	23.19	5.346	13.97	9.65	HOMO-1→LUMO+2	20	
									HOMO-1→LUMO+4	4	
									HOMO-1→LUMO+5	2	
									HOMO-1→LUMO+8	5	
									HOMO→LUMO+2	29	
									HOMO→LUMO+4	5	
	HOMO→LUMO+5	4									
	HOMO→LUMO+8	10									
	26	327.48	3.78	0.21	23.19	5.346	13.97	9.65	3.88	HOMO-9→LUMO+2	4
										HOMO-1→LUMO	7
										HOMO-1→LUMO+2	15
										HOMO-1→LUMO+5	4
										HOMO→LUMO	6
										HOMO→LUMO+4	7
	HOMO→LUMO+5	11									
	HOMO→LUMO+8	4									
	HOMO→LUMO+17	2									
	HOMO→LUMO+19	6									
<b>9, ref</b>	2	421	3.25	2.15	15.23	-	5.2	4.78 <sup>a</sup>	-	-	

<sup>a</sup> The value is charge-transfer distance ( $d_{CT}$ ) which measures the distance between the barycenters of density gain and depletion upon excitation.<sup>[117]</sup>



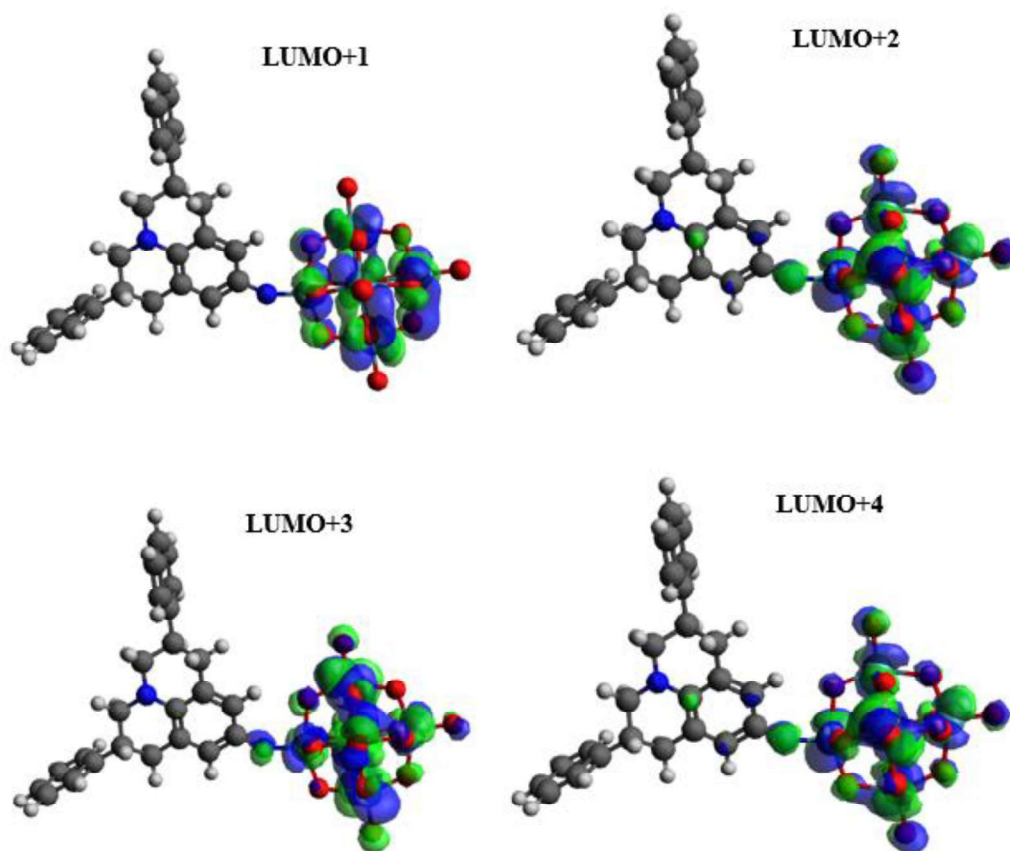
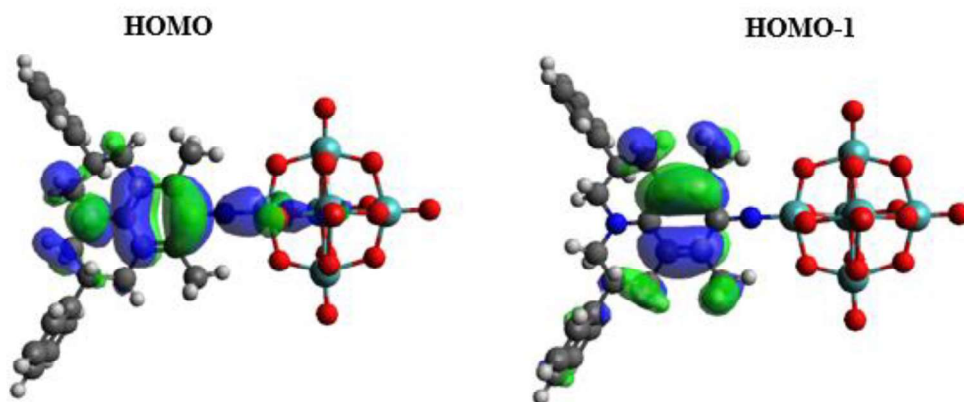
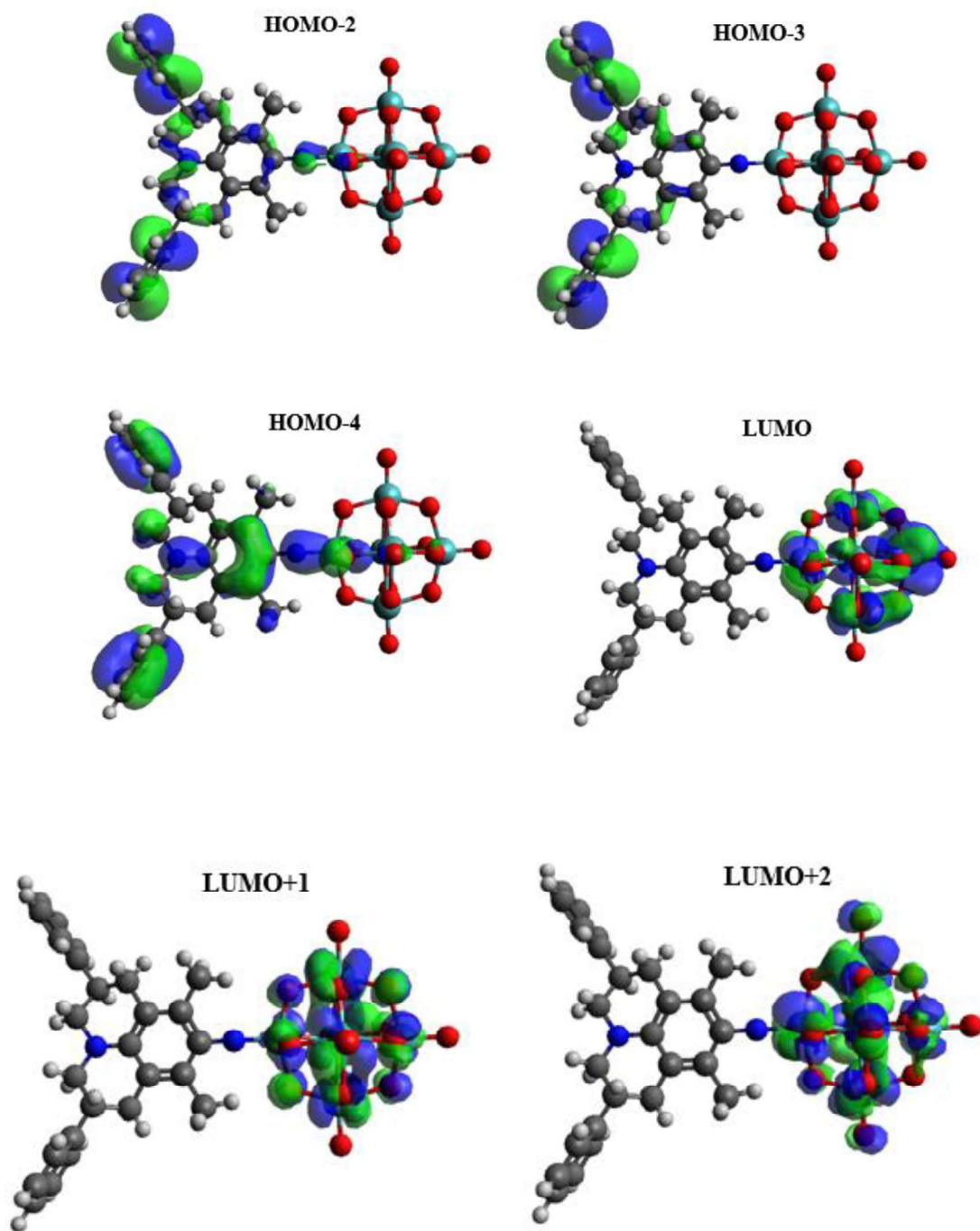


Figure 3.10 The molecular orbitals involved in significant transitions of 5.





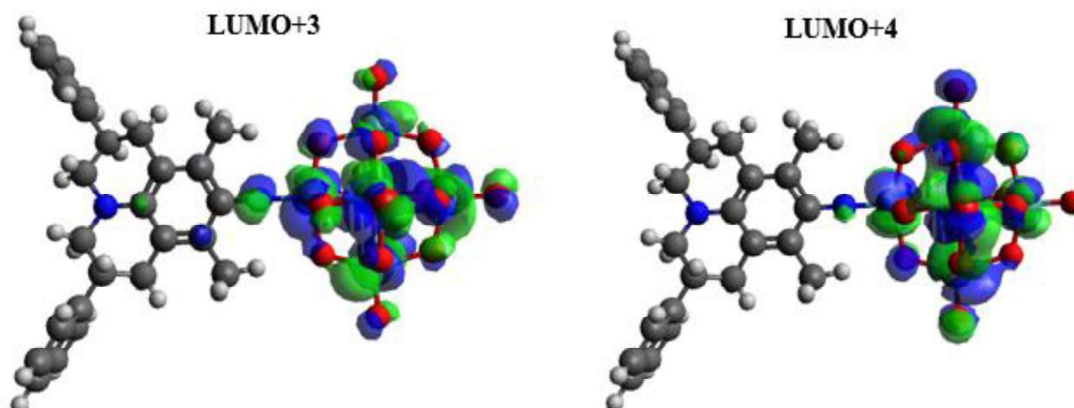
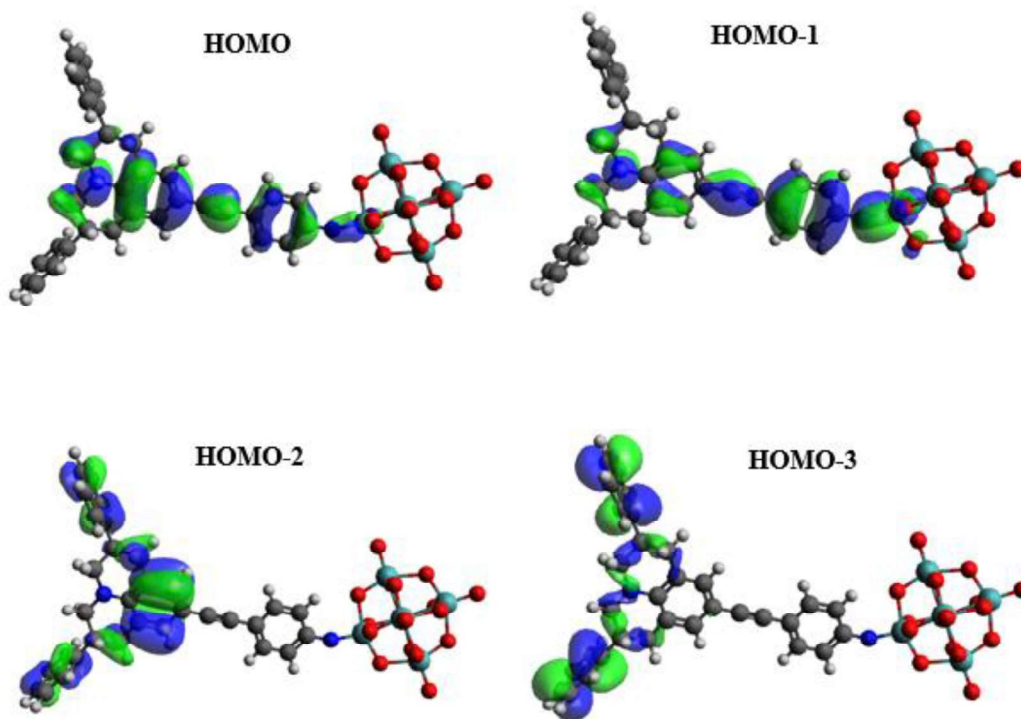


Figure 3.11 The molecular orbitals involved in significant transitions of 6.





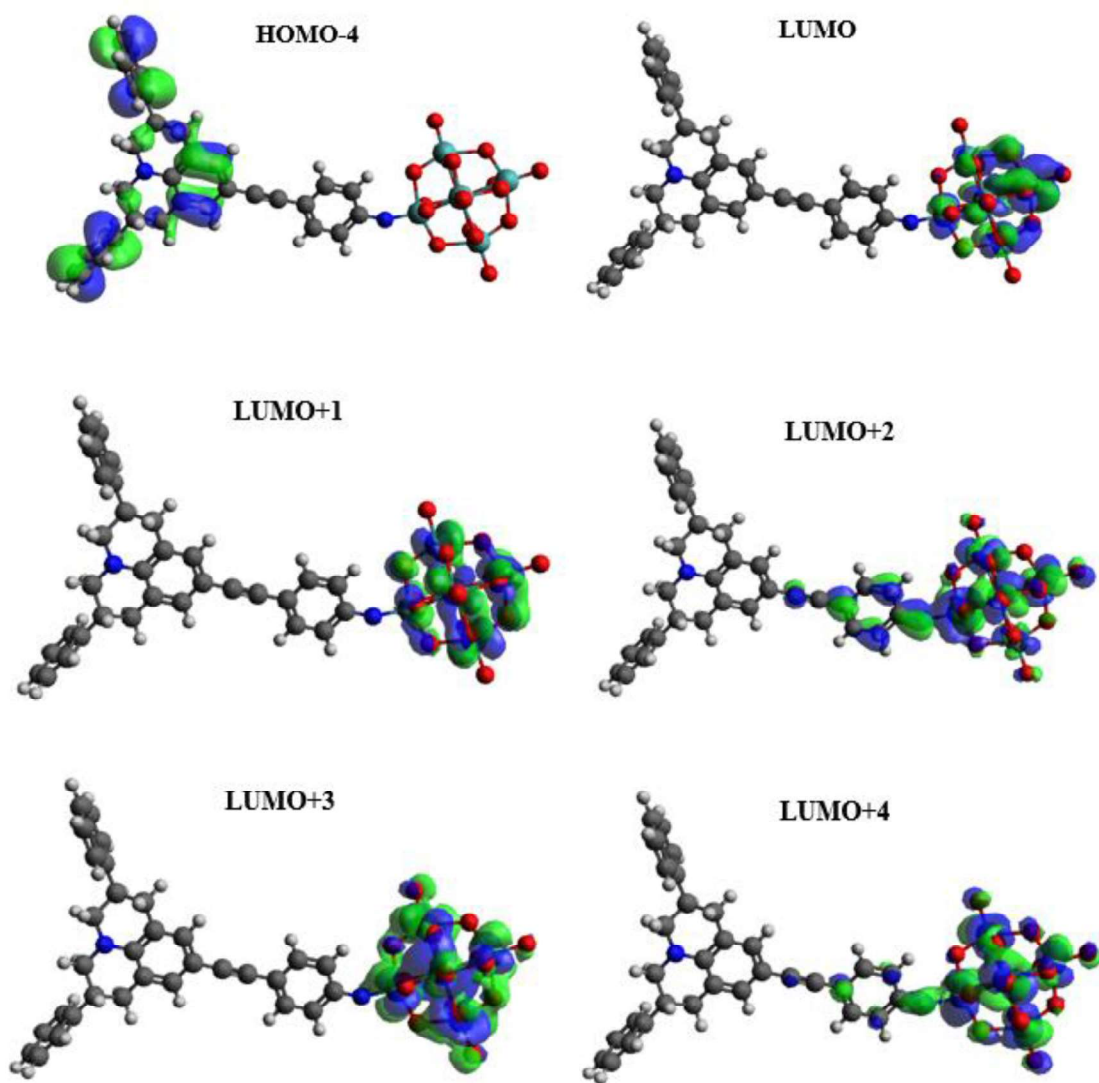
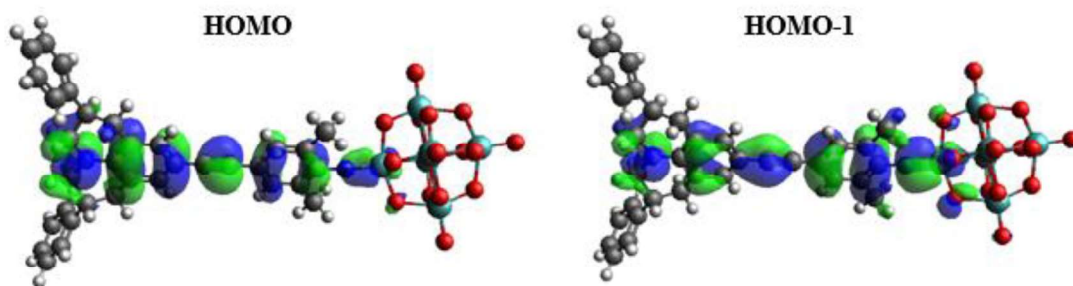


Figure 3.12 The molecular orbitals involved in significant transitions of 7



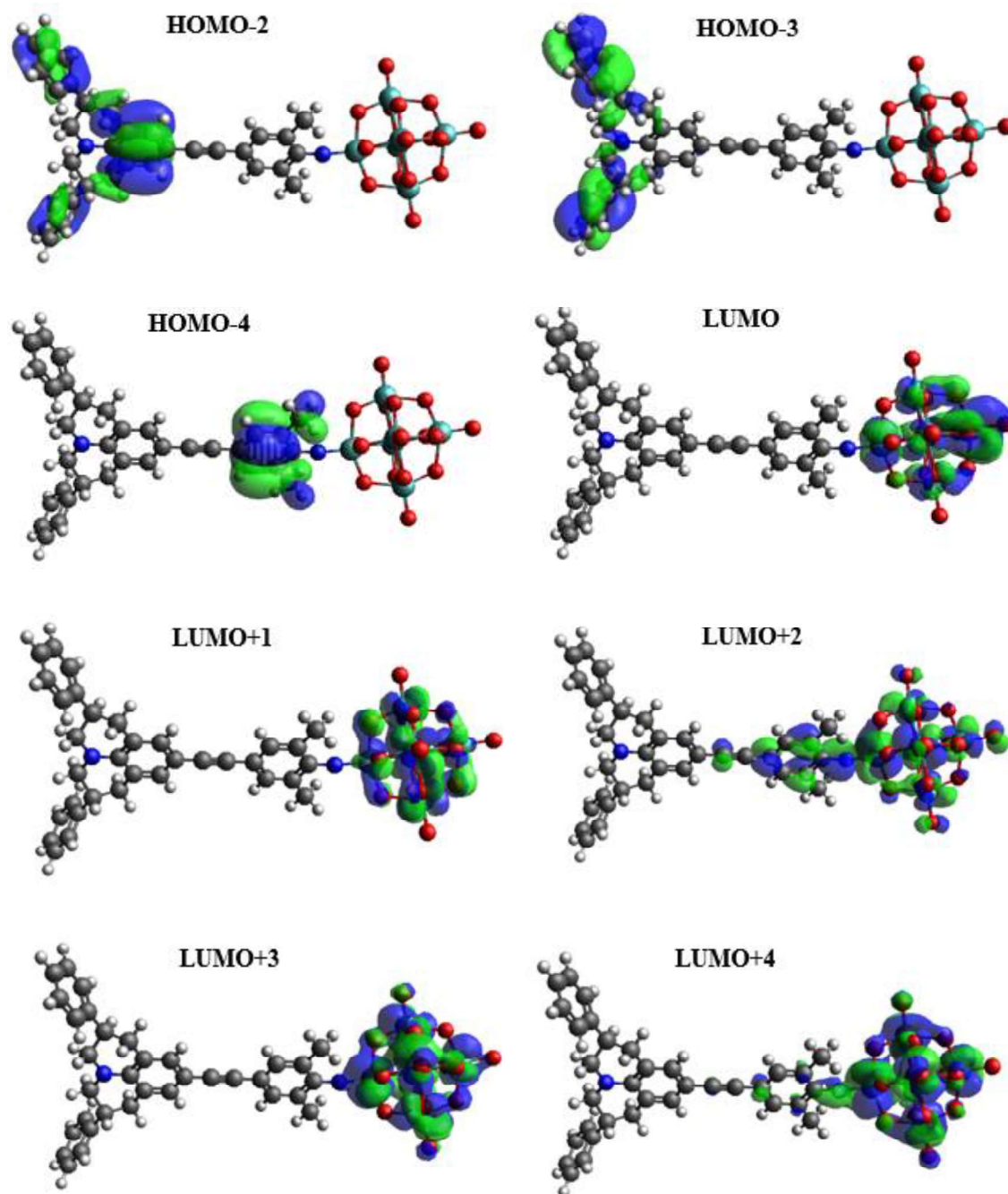


Figure 3.13 The molecular orbitals involved in significant transitions of 8.

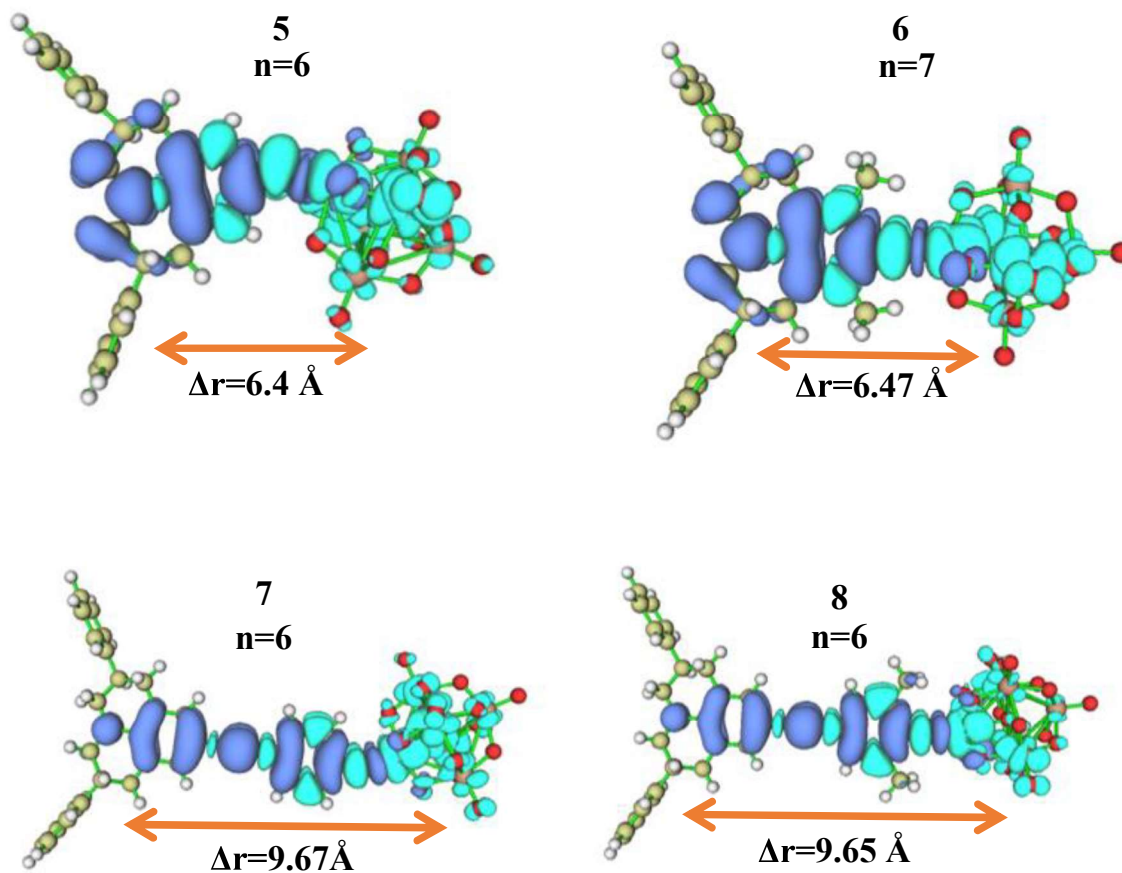


Figure 3.14 Excitation-induced charge density difference ( $\Delta r$ ) for key excited states of compounds 5-8 (isovalue = 0.0003 au; light/dark blue corresponds to positive/negative  $\Delta r$  so that the excitation-induced electron transfer goes from dark to light blue).

### 3.5 Conclusion:

- 1- Using DFT/TD-DFT calculations, a novel set of Lindqvist-type hexamolybdate organoimido POMs derivatized with julolidine donor groups have been examined as second-order NLO compounds.



- 2- The findings indicate a significant improvement in the first hyperpolarizabilities, which could be ascribed to the donor strength of julolidine while maintaining basically the same transparency window.
- 3- In comparison to the short compounds, the extension of the  $\pi$ -conjugated linker (phenylacetylene spacer) raises values by a factor of 2.1 while keeping nearly identical electronic transition energies.
- 4- The significant excitation-induced electron transfers and dipoles moment change from the julolidine to the hexamolybdate were responsible for the increased second-order NLO activity.
- 5- Although this decreases the first hyperpolarizability, ortho-methylation to the imido-bond has a substantial impact on the stability, and consequently the length and uniformity, of the bond.

### 3.6 Future Works:

This study demonstrates the superior NLO activity for julolidine-POM materials and future works could include the following:

- 1- The findings could motivate experimentalist to synthesis these materials and studying their NLO properties.
- 2- Further tailoring of the julolidine donor (substituents) and studying the tuning effects on the NLO activity.
- 3- Alteration of the POM types (Keggin, Anderson, etc.) and hence studying the acceptor strength on the NLO responses.
- 4- Investigation of redox switching characteristics are already in process

## References:

- [1] A. Al-Yasari, Synthesis, non-linear optical and electrochemical properties of novel organoimido polyoxometalate derivatives ,**2016**, 221.
- [2] P. E. Powers, Fundamentals of Nonlinear, Optics *Linear Optics*, **2020**.
- [3] P. A. Franken, A. E. Hill, C. W. Peters, G. Weinreich, *Phys. Rev. Lett.* **1961**, 7, 118.
- [4] R. W. Boyd, *The Nonlinear Optical Susceptibility*, **2020**.
- [5] M. Moshinsky, *Handbook of Advanced Electronic and Photonic Materials and Devices*, Vol. 13, **1959**.
- [6] P. C. Ray, *Chem. Rev.* **2010**, 110, 5332.
- [7] S. Muhammad, H. L. Xu, R. L. Zhong, Z. M. Su, A. G. Al-Sehemi, A. Irfan, *J. Mater. Chem. C* **2013**, 1, 5439.
- [8] S. Semin, X. Li, Y. Duan, T. Rasing, *Adv. Opt. Mater.* **2021**, 9.
- [9] S. Bai, D. Wang, H. Liu, Y. Wang, *Inorg. Chem. Front.* **2021**, 8, 1637.
- [10] J. L. Oudar, D. S. Chemla, *Opt. Commun.* **1975**, 13, 164.
- [11] J. W. Zhao, J. L. Zhang, Y. Z. Li, J. Cao, L. J. Chen, *Cryst. Growth Des.* **2014**, 14, 1467.
- [12] T. P. Radhakrishnan, *Acc. Chem. Res.* **2008**, 41, 367.
- [13] M. U. Khan, M. Khalid, M. Ibrahim, A. A. C. Braga, M. Safdar, A. A. Al-Saadi, M. R. S. A. Janjua, *J. Phys. Chem. C* **2018**, 122, 4009.
- [14] A. Cesaretti, P. Foggi, C. G. Fortuna, F. Elisei, A. Spalletti, B. Carlotti, *J. Phys. Chem. C* **2020**, 124, 15739.
- [15] A. Al-Yasari, P. Spence, H. El Moll, N. Van Steerteghem, P. N. Horton, B. S. Brunshawig, K. Clays, J. Fielden, *Dalt. Trans.* **2018**, 47, 10415.

- [16] C. G. Liu, M. L. Gao, Z. J. Wu, *RSC Adv.* **2014**, *4*, 38300.
- [17] T. Isophorone, X. Huang, Z. Li, M. Peng, Z. Zeng, Z. Huang, F. Liu, X. Chen, **2022**.
- [18] P. Norman, K. Ruud, *Non-Linear Opt. Prop. Matter* **2006**, *1*.
- [19] M. U. Khan, M. Ibrahim, M. Khalid, A. A. C. Braga, S. Ahmed, A. Sultan, *J. Clust. Sci.* **2019**, *30*, 415.
- [20] R. Tang, S. Zhou, Z. Cheng, G. Yu, Q. Peng, H. Zeng, G. Guo, Q. Li, Z. Li, *Chem. Sci.* **2016**, *8*, 340.
- [21] W. Wu, L. Huang, L. Xiao, Q. Huang, R. Tang, C. Ye, J. Qin, Z. Li, *RSC Adv.* **2012**, *2*, 6520.
- [22] S. R. Marder, L. T. Cheng, B. G. Tiemann, A. C. Friedli, M. Blanchard-Desce, J. W. Perry, J. Skindhøj, *Science (80-. )*. **1994**, *263*, 511.
- [23] J. Luo, F. Lin, Z. Li, M. Li, T. D. Kim, S. H. Jang, A. K. Y. Jen, *J. Mater. Chem. C* **2017**, *5*, 2230.
- [24] Y. Chen, Y. Zhang, Y. Shen, Y. Yao, Y. Zhao, Y. Q. Qiu, *New J. Chem.* **2021**, *45*, 10725.
- [25] Y. Shen, X. Li, J. Ye, Y. Qiu, *Comput. Theor. Chem.* **2019**, *1163*, 112535.
- [26] Y. X. Hu, X. Xia, W. Z. He, Z. J. Tang, Y. L. Lv, X. Li, D. Y. Zhang, *Org. Electron.* **2019**, *66*, 126.
- [27] S. Di Bella, A. Colombo, C. Dragonetti, S. Righetto, D. Roberto, *Inorganics* **2018**, *6*.
- [28] C. Koos, J. Leuthold, W. Freude, M. Kohl, L. Dalton, W. Bogaerts, A. L. Giesecke, M. Lauermann, A. Melikyan, S. Koeber, S. Wolf, C. Weimann, S. Muehlbrandt, K. Koehnle, J. Pfeifle, W. Hartmann, Y. Kutuvantavida, S. Ummethala, R. Palmer, D. Korn, L. Alloatti, P. C. Schindler, D. L.

- Elder, T. Wahlbrink, J. Bolten, *J. Light. Technol.* **2016**, *34*, 256.
- [29] Y. He, L. Chen, H. Zhang, Z. Chen, F. Huo, B. Li, Z. Zhen, X. Liu, S. Bo, *J. Mater. Chem. C* **2018**, *6*, 1031.
- [30] X. Zang, G. Liu, Q. Li, Z. Li, Z. Li, *Macromolecules* **2020**, *53*, 4012.
- [31] D. Marpaung, J. Yao, J. Capmany, *Nat. Photonics* **2019**, *13*, 80.
- [32] M. Wielopolski, J. H. Kim, Y. S. Jung, Y. J. Yu, K. Y. Kay, T. W. Holcombe, S. M. Zakeeruddin, M. Grätzel, J. E. Moser, *J. Phys. Chem. C* **2013**, *117*, 13805.
- [33] S. Namuangruk, R. Fukuda, M. Ehara, J. Meeprasert, T. Khanasa, S. Morada, T. Kaewin, S. Jungstittiwong, T. Sudyoadsuk, V. Promarak, *J. Phys. Chem. C* **2012**, *116*, 25653.
- [34] M. Khalid, A. Ali, R. Jawaria, M. A. Asghar, S. Asim, M. U. Khan, R. Hussain, M. Fayyaz ur Rehman, C. J. Ennis, M. S. Akram, *RSC Adv.* **2020**, *10*, 22273.
- [35] Y. Bai, Z. J. Zhou, J. J. Wang, Y. Li, D. Wu, W. Chen, Z. R. Li, C. C. Sun, *J. Phys. Chem. A* **2013**, *117*, 2835.
- [36] K. Shehzadi, K. Ayub, T. Mahmood, *Appl. Surf. Sci.* **2019**, *492*, 255.
- [37] J. Liu, G. Xu, F. Liu, I. Kityk, X. Liu, Z. Zhen, *RSC Adv.* **2015**, *5*, 15784.
- [38] A. Al-Yasari, N. Van Steerteghem, H. El Moll, K. Clays, J. Fielden, *Dalt. Trans.* **2016**, *45*, 2818.
- [39] P. J. Mendes, T. J. L. Silva, M. H. Garcia, J. P. P. Ramalho, A. J. P. Carvalho, *J. Chem. Inf. Model.* **2012**, *52*, 1970.
- [40] A. Avramopoulos, R. Zalesny, H. Reis, M. G. Papadopoulos, *J. Phys. Chem. C* **2020**, *124*, 4221.

- [41] E. C. Harvey, B. L. Feringa, J. G. Vos, W. R. Browne, M. T. Pryce, *Coord. Chem. Rev.* **2015**, 282–283, 77.
- [42] S. Muhammad, S. Kumar, J. Koh, M. Saravanabhavan, K. Ayub, M. Chaudhary, *Mol. Simul.* **2018**, 44, 1191.
- [43] C. Joachim, Electronics using hybrid-molecular and mono-molecular devices, **2000**, 541.
- [44] J. R. Heath, M. A. Ratner, *Phys. Today* **2003**, 43.
- [45] V. Wijnkoop, U. A. Sai, V. Amsterdam, **1990**, 8, 2345.
- [46] S. Liu, Z. Tang, *Nano Today* **2010**, 5, 267.
- [47] P. I. T. A. C. O. I. C. A. THEIR, 2005] APPLICATIONS, BIOMEDICAL.[Frontiers in Bioscience 10, 275--287, January 1, **2005**, 275.
- [48] P. Gouzerh, M. Che, *Actual. Chim.* **2006**, 9.
- [49] Z. Lang, DFT Studies on Polyoxopalladates and Polyoxometalate-surface Composites: From Structure to Catalysis, **2017**.
- [50] H. R. Allcock, E. C. Bissell, E. T. Shawl, R. J. I. I, **1973**, 12.
- [51] M. Haroon, M. R. S. A. Janjua, *Mater. Today Commun.* **2021**, 26, 101880.
- [52] J. Kang, B. Xu, Z. Peng, X. Zhu, Y. Wei, D. R. Powell, *Angew. Chemie - Int. Ed.* **2005**, 44, 6902.
- [53] L. Yan, M. Jin, P. Song, Z. Su, *J. Phys. Chem. B* **2010**, 114, 3754.
- [54] Y. Du, E. A. Maatta, A. L. Rheingold, *J. Am. Chem. Soc.* **1992**, 114, 345.
- [55] L. Xu, M. Lu, B. Xu, Y. Wei, Z. Peng, D. R. Powell, *Angew. Chemie - Int. Ed.* **2002**, 41, 4129.
- [56] M. Lu, Y. Wei, B. Xu, C. F. C. Cheung, Z. Peng, D. R. Powell, *Angew.*

*Chemie - Int. Ed.* **2002**, *41*, 1566.

- [57] M. Haroon, M. R. S. A. Janjua, *J. Phys. Org. Chem.* **2022**, *35*, 1.
- [58] J. B. Strong, G. P. A. Yap, R. Ostrander, L. M. Liable-sands, A. L. Rheingold, P. Gouzerh, E. A. Maatta, M. Curie, **2000**, 639.
- [59] T. R. Mohs, Y. Du, B. Plashko, E. A. Maatta, *Chem. Commun.* **1997**, *18*, 1707.
- [60] J. Zhang, F. Xiao, J. Hao, Y. Wei, *Dalt. Trans.* **2012**, *41*, 3599.
- [61] and R. W. Likai Yan, Guochun Yang, Wei Guan, Zhongmin Su, *J. Phys. Chem. B* **2005**, *109*, 22332.
- [62] L. Yan, G. Yang, W. Guan, Z. Su, R. Wang, *J. Phys. Chem. B* **2005**, *109*, 22332.
- [63] R. J. Errington, S. S. Petkar, P. S. Middleton, W. McFarlane, W. Clegg, R. A. Coxall, R. W. Harrington, *J. Am. Chem. Soc.* **2007**, *129*, 12181.
- [64] W. W. Ju, H. T. Zhang, X. Xu, Y. Zhang, Y. Xu, *Inorg. Chem.* **2014**, *53*, 3269.
- [65] T. Polyoxotungstate, W. Guan, G. Yang, L. Yan, Z. Su, **2006**, *45*, 7864.
- [66] B. Xu, Y. Wei, C. L. Barnes, Z. Peng, *Angew. Chemie - Int. Ed.* **2001**, *40*, 2290.
- [67] B. Xu, M. Lu, J. Kang, D. Wang, J. Brown, Z. Peng, *Chem. Mater.* **2005**, *17*, 2841.
- [68] J. Zhuang, L. Yan, C. Liu, Z. Su, *Eur. J. Inorg. Chem.* **2009**, 2529.
- [69] P. Song, C. Liu, W. Guan, L. Yan, X. Sun, C. Yao, Z. Su, *Can. J. Chem.* **2011**, *89*, 61.
- [70] A. Al-Yasari, N. Van Steerteghem, H. Kearns, H. El Moll, K. Faulds, J. A.

- Wright, B. S. Brunschwig, K. Clays, J. Fielden, *Inorg. Chem.* **2017**, *56*, 10181.
- [71] A. Al-Yasari, H. El Moll, R. Purdy, K. B. Vincent, P. Spence, J. P. Malval, J. Fielden, *Phys. Chem. Chem. Phys.* **2021**, *23*, 11807.
- [72] E. Rtibi, M. Abderrabba, S. Ayadi, B. Champagne, *Inorg. Chem.* **2019**, *58*, 11210.
- [73] E. Rtibi, B. Champagne, *Symmetry (Basel)*. **2021**, *13*, 1636.
- [74] P. A. D. S. Abranches, W. F. De Paiva, Â. De Fátima, F. T. Martins, S. A. Fernandes, *J. Org. Chem.* **2018**, *83*, 1761.
- [75] Š. Budzák, D. Jacquemin, *Phys. Chem. Chem. Phys.* **2018**, *20*, 25031.
- [76] A. R. Katritzky, B. Rachwal, S. Rachwal, K. A. Abboud, *J. Org. Chem.* **1996**, *61*, 3117.
- [77] D. Bai, A. C. Benniston, S. Clift, U. Baisch, J. Steyn, N. Everitt, P. Andras, *J. Mol. Struct.* **2014**, *1065–1066*, 10.
- [78] M. Zheng, H. Tang, L. Li, Q. Hu, L. Zhang, H. Xue, H. Pang, *Adv. Sci.* **2018**, *5*.
- [79] J. Wu, J. Liu, T. Zhou, S. Bo, L. Qiu, Z. Zhen, X. Liu, *RSC Adv.* **2012**, *2*, 1416.
- [80] C. Hu, Z. Chen, H. Xiao, Z. Zhen, X. Liu, S. Bo, *J. Mater. Chem. C* **2017**, *5*, 5111.
- [81] J. Wu, W. Wang, N. Wang, J. He, G. Deng, Z. Li, X. Zhang, H. Xiao, K. Chen, *Phys. Chem. Chem. Phys.* **2018**, *20*, 23606.
- [82] G. Wu, F. Kong, J. Li, W. Chen, X. Fang, C. Zhang, Q. Chen, X. Zhang, S. Dai, *Dye. Pigment.* **2013**, *99*, 653.

- [83] A. Nano, M. P. Gullo, B. Ventura, N. Armaroli, A. Barbieri, R. Ziessel, *Chem. Commun.* **2015**, *51*, 3351.
- [84] G. Martini, E. Martinelli, G. Ruggeri, G. Galli, A. Pucci, *Dye. Pigment.* **2015**, *113*, 47.
- [85] Z. Xia, X. Guo, Y. Zhu, Y. Wang, J. Wang, *RSC Adv.* **2018**, *8*, 13588.
- [86] M. Zhang, H. Xu, M. Fu, M. Yang, B. He, X. Zhang, Z. Li, G. Deng, S. Bo, J. Liu, *New J. Chem.* **2019**, *43*, 15548.
- [87] E. Schrödinger, *Phys. Rev.* **1926**, *28*, 1049.
- [88] R. A. Friesner, *Proc. Natl. Acad. Sci. U. S. A.* **2005**, *102*, 6648.
- [89] H. Akbas, O. T. Turgut, *J. Math. Phys.* **2018**, *59*.
- [90] S. R. G. Fernando, Computational Studies on Bimetallic Catalysis and X-ray Absorption Spectroscopy, **2015**.
- [91] Fabiana Meijon Fadul, Modeling Friction, Wear and Lubrication of Sliding Polyurethane and Polycarbonate Surfaces Representing Printer Components with Molecular Dynamics, **2019**.
- [92] Developing Entangled Two-Photon Absorption for Unique Control of Exciting Organic, C. A. E. and T. Approach, *Suparyanto dan Rosad (2015)* **2020**, *5*, 248.
- [93] C. J. Cramer, *Essentials of Computational Chemistry, Second Edition*, **2004**.
- [94] M. Travis, Modeling Transition Metal Catalysts for Small Molecule Activation and Functionalization, **2013**.
- [95] B. H. Lei, Z. Yang, H. Yu, C. Cao, Z. Li, C. Hu, K. R. Poepelmeier, S. Pan, *J. Am. Chem. Soc.* **2018**, *140*, 10726.



- [96] W. Cui, J. Chen, *Int. J. Min. Sci. Technol.* **2021**, *31*, 983.
- [97] M. R. S. A. Janjua, W. Guan, C. G. Liu, S. Muhammad, L. Yan, Z. Su, *Eur. J. Inorg. Chem.* **2009**, 5181.
- [98] P. Krawczyk, *J. Mol. Model.* **2015**, *21*.
- [99] T. Körzdörfer, J. L. Brédas, *Acc. Chem. Res.* **2014**, *47*, 3284.
- [100] S. Baroni, R. Gebauer, *The Liouville-Lanczos Approach to ( Perturbation ) Theory*, **2012**.
- [101] D. Mester, K. Mihaly, *J. Chem. Theory Comput.* **2021**, *17*, 927.
- [102] É. Brémond, Á. J. Pérez-Jiménez, J. C. Sancho-García, C. Adamo, *J. Chem. Phys.* **2020**, *152*.
- [103] Y. Kurzweil, K. V. Lawler, M. Head-Gordon, *Mol. Phys.* **2009**, *107*, 2103.
- [104] J. Da Chai, M. Head-Gordon, *Phys. Chem. Chem. Phys.* **2008**, *10*, 6615.
- [105] R. Johnson, *Theoretical Studies of Transition Metal Catalysis*, **2014**.
- [106] T. Rogova, *Appl. Mater. Interfaces* **2022**.
- [107] F. Jensen, *Introduction to Computational Chemistry*, **2007**.
- [108] M. Dolg, H. Stoll, H. Preuss, *J. Chem. Phys.* **1989**, *90*, 1730.
- [109] T. R. Cundari, W. J. Stevens, *J. Chem. Phys.* **1993**, *98*, 5555.
- [110] P. J. Hay, W. R. Wadt, *J. Chem. Phys.* **1985**, *82*, 299.
- [111] S. Chiodo, N. Russo, E. Sicilia, *J. Chem. Phys.* **2006**, *125*.
- [112] Y. Yang, M. N. Weaver, K. M. Merz, *J. Phys. Chem. A* **2009**, *113*, 9843.
- [113] T. Lu, F. Chen, *J. Comput. Chem.* **2012**, *33*, 580.
- [114] C. A. Guido, P. Cortona, B. Mennucci, C. Adamo, *J. Chem. Theory*

*Comput.* **2013**, *9*, 3118.

[115] R. Bersohn, P. A. O. Yoh-Han, H. L. Frisch, *J. Chem. Phys.* **1966**, *45*, 3184.

[116] E. Rtibi, B. Champagne, *Symmetry (Basel)*. **2021**, *13*.

[117] T. Le Bahers, C. Adamo, I. Ciofini, *J. Chem. Theory Comput.* **2011**, *7*, 2498.

## الخلاصة

تقسم هذه الاطروحة الى ثلاث أقسام: الاول تضمن مقدمة عن مواد NLO وكيفية توليد SHG مع شرح على الربط بين المانح والمستقبل والربط بينهما من خلال  $\pi$ -bridges بواسطة Two-State Model وكذلك تم التطرق على POM مع انواعه وايضاً تم توضيح عن أقوى مانح موجود وهو الجولودين. في القسم الثاني تم ايضاح معادلة شرودنجر والتقريبات الاربعة وماهية كيمياء الكم وما هو HF بعدها تم التكلم عن TDDFT و DFT والمواضيع ذات الصلة. في القسم الثالث كانت مناقشة لجميع النتائج التي تم الحصول عليها.

تستخدم المواد البصرية غير الخطية لمعالجة ضوء الليزر من خلال ظواهر من الدرجة الثانية مثل التوليد التوافقي الثاني (مضاعفة التردد) وتأثيرات الدرجة الثالثة على سبيل المثال امتصاص فوتونات متعددة. في هذه الرسالة يتم التحقق في مواد حيث يتم توصيل مستقبلات الالكترن POM عبر مجموعات مانحه الالكترن العضوي في هذا المشروع قمنا من الناحية النظرية من خلال حسابات نظرية كثافة الدالة في الغالب بدراسات المركبات الجديدة بشكل منهجي مثل مجموعات المانحة Julolidine القوية للمركبات اللاخطية الضوئية الفعالة كما تم تقييم الهياكل الهندسية والالكترونية والخصائص البصرية وغير الخطية التربيعية من خلال ادخال Julolidine فيها وتظهر الأنظمة المدروسة استجابات غير خطية كبيرة من الدرجة الثانية

$1048 \times 10^{-30}$  esu للمركب 3 عند تعزيز الرابطة المقترنة يتم تحسين استجابات المحسوبة بمعامل 2.1 كما تم فحص اثار التعويض (مجموعات الالكيل والفينيل) على فاعلية مانح Julolidine وبالتالي على الاستجابات اظهرت النتائج زيادة في الاستجابة لمشتقات Julolidine المعوضة للفينيل كما أظهرت النتائج تعزيزا يصل الى 2.1 في استجابات  $\beta$  لمشتقات Julolidine المستبدلة بالفينيل التي تصل الى  $10^{-30} \times$  1048esu للمركب 8.

بشكل عام تشير حسابات TDDFT الى ان الانتقال قوي منخفض الطاقة يمكن ان يعزى بشكل أساسي الى نقل الشحنة من Julolidine -اريل اميدو الى مجموعة hexamolybdate مما يشير الى وجود اتصال قوي بين مكونات POM و Julolidine المسؤولة عن السلوك الخطي الغير بصري لخطوط هذه المركبات. بالنسبة لرابطة مثلية اورثو اميدو لها تأثير كبير على الاستقرار وبالتالي طول وخطية الرابطة على الرغم من انها تقلل بشكل طفيف قيمة بيتا. تظهر المجموعة الكاملة من النتائج نشاط المواد اللاخطية الضوئية لمركبات POM و Julolidine مع الحفاظ على نافذة شفافية جيدة نسبيا مقارنة بالأنظمة العضوية النقية المماثلة.



جامعة كربلاء

كلية العلوم

قسم الكيمياء

دراسة الخواص الضوئية والكهروكيميائية لمركبات بولييمرات اكاسيد  
الفلزات كمركبات ضوئية لاختية

رسالة مقدمة الى مجلس كلية العلوم / جامعة كربلاء وهي جزء من متطلبات  
نيل درجة الماجستير في علوم الكيمياء

من قبل

أشرف حسين صالح

بإشراف

أ.م.د. حسن فيصل نعمة

أ.م.د. أحمد هادي اليساري